Title

GJA1 Depletion Causes Ciliary Defects by Affecting Rab11 Trafficking to the Ciliary Base

Author names and affiliations

Dong Gil Jang[1], Keun Yeong Kwon[1], Yeong Cheon Kweon[1], Byung-gyu Kim[2], Kyungjae Myung[2], Hyun-Shik Lee[3], Chan Young Park[1], Taejoon Kwon[2,4,*] and Tae Joo Park[1,2,*]

[1] Department of Biological Sciences, College of Information-Bio Convergence Engineering, Ulsan National Institute of Science and Technology, Ulsan 44919, Republic of Korea

[2] Center for Genomic Integrity, Institute for Basic Science, Ulsan 44919, Republic of Korea

[3] KNU-Center for Nonlinear Dynamics, CMRI, School of Life Sciences, BK21 Plus KNU Creative Bio Research Group, College of Natural Sciences, Kyungpook National University, Daegu 41566, Republic of Korea

[4] Department of Biomedical Engineering, College of Information-Bio Convergence Engineering, Ulsan National Institute of Science and Technology, Ulsan 44919, Republic of Korea

[*] Corresponding author

Abstract

The gap junction complex functions as a transport channel across the membrane. Among gap junction subunits, gap junction protein α1 (GJA1) is the most commonly expressed subunit. A recent study showed that GJA1 is necessary for the maintenance of motile cilia; however, the molecular mechanism and function of GJA1 in ciliogenesis remain unknown. Here, we examined the functions of GJA1 during ciliogenesis in human retinal pigment epithelium-1 and *Xenopus laevis* embryonic multiciliated-cells. GJA1 localizes to the motile ciliary axonemes or pericentriolar regions beneath the primary cilium. GJA1 depletion caused malformation of both the primary cilium and motile cilia. Further study revealed that GJA1 depletion affected several ciliary proteins such as BBS4, CP110, and Rab11 in the pericentriolar region and basal body. Interestingly, CP110 removal from the mother centriole was significantly reduced by GJA1 depletion. Importantly, Rab11, a key regulator during ciliogenesis, was immunoprecipitated with GJA1, and GJA1 knockdown caused the mislocalization of Rab11. These findings suggest that GJA1 regulates ciliogenesis by interacting with the Rab11-Rab8 ciliary trafficking pathway.

Introduction

A gap junction, which is also known as a connexon, is a transmembrane (TM) protein complex that plays an important role as a channel and transports low-molecular-weight compounds, nutrients, and ions laterally across the plasma membrane [1, 2]. It also regulates cell proliferation, differentiation, growth, and death [3-5]. A gap junction is composed of gap junction protein subunits, and five subgroups of gap junction protein families have been classified according to their amino acid sequence homology [6]. Twelve gap junction proteins comprise a gap junction complex, which consists of a combination of 21 human gap junction proteins [7].

Gap junction protein α1 (GJA1), also known as connexin 43 (CX43, 43 kDa), was originally identified in the rat heart [8]. The human homolog of GJA1 is located at human chromosome 6q22-q23. The GJA1 gene was identified after discovering the putative genes for human oculodentodigital dysplasia (ODDD) [9, 10]. Among all gap junction protein families, GJA1 is the most common and is a major subunit. It is expressed in many tissues, such as the eyes, ears, brain, and especially the heart [11-14].

The GJA1 protein has four TM domains with five linked subdomain loops. Among these loops, two loops are extracellular subdomains, and three loops, including the N- and C-terminal domains, are in the cytoplasm (Fig 1A) [15]. In the cytoplasm, the C-terminal domain of GJA1 regulates the cytoskeletal network (actin and tubulin [16]) and cell extension, migration, and polarity [17-19]. A recent study reported that GJA1 also regulates the maintenance of cilia [20], which are microtubule-based cellular organelles that play crucial roles in the physiological maintenance of the human body [21]. However, the molecular mechanisms and roles of GJA1 in the formation and function of cilia have not been determined.

Cilia exist in most types of vertebrate cells and are involved in various developmental processes and physiological responses from embryos to adults. For example, cilia are involved in cell cycle control, cell-to-cell signal transduction, fertilization, early embryonic development, extracellular environment sensing, and homeostasis [22]. Mutations in essential genes for cilia formation disrupt ciliary structures or their functions and lead to “ciliopathy”, which is an innate genetic and syndromic disorder [23, 24].

In this report, we show that GJA1 regulates ciliogenesis by affecting ciliary trafficking and thereby promoting uncapping of the mother centriole. GJA1 is localized not only at the gap junction but also in the pericentriolar regions beneath the primary cilium of retinal pigment epithelium-1 (RPE1) cells and the ciliary axonemes of multiple/motile cilia.

Using immunoprecipitation-mass spectrometry (IP-MS) analysis, we identified Rab11 and Rab8a as

putative GJA1-binding partners. Rab11 was previously shown to accumulate around the basal body and is involved in the early steps of ciliogenesis [25, 26]. Further analysis showed that Rab11 immunoprecipitated with GJA1, and knockdown of GJA1 in RPE1 cells resulted in the mislocalization of Rab11. These data suggest that GJA1 contributes to proper ciliogenesis by regulating Rab11 trafficking to basal bodies and facilitating ciliary axoneme formation and assembly.

Results

1. GJA1 is localized at the ciliary axonemes and near the basal bodies in multiciliated cells.

GJA1, which is a major component of the gap junction complex, consists of four TM domains (TM1–4), interdomain loops between each TM domain, and intracellular N- and C-terminus domains (Fig 1A). To investigate the biological effects of GJA1 on ciliogenesis in vertebrates, we cloned the *Xenopus laevis* homolog of human GJA1 based on a sequence from the Xenbase database [27]. Next, we analyzed GJA1 localization in multiciliated cells in *Xenopus* embryos expressing GJA1-Flag or HA-tagged protein by immunofluorescence staining. We observed that GJA1-Flag strongly accumulated at the cell-cell junction as a gap junction complex (Fig 1B, white arrowhead). Unexpectedly, we also observed that GJA1 was localized near the apical surface as puncta (Fig 1B, 1B', yellow arrow) and in ciliary axonemes (Fig 1C, 1C', white arrow), in addition to gap junctions in *Xenopus* multiciliated epithelial cells. We further analyzed apical localization of GJA1 puncta by co-immunostaining with a basal body marker, centrin. Interestingly, GJA1-HA signals did not overlap with centrin signals. Instead, GJA1-HA was localized below or above the basal bodies (Fig 1D, 1D', Fig S1A). Additionally, we examined the endogenous GJA1 location in multiciliated cells in the mouse branchial epithelium and found that endogenous GJA1 localizes to the ciliary axonemes as puncta (Fig S1B). These data suggest that GJA1 may be involved in ciliogenesis.

2. Dominant-negative mutant-mediated dysfunction of GJA1 causes severe ciliary malformation in *Xenopus* embryonic epithelial tissue.

To determine the function of GJA1 during cilia formation, we exploited dominant-negative mutants of GJA1 (dnGJA1). Two known dominant-negative mutants have been identified and were used in recent studies. The T154A point mutation mimics the closed-channel status of the gap junction complex but does not inhibit gap junction formation [28]. The Δ130–136 deletion mutation consists of a seven-amino acid deletion in the intracellular loop between TM2 and 3 that blocks gap junction permeability [29]. Lastly, we designed the Δ234–243 mutant, which consists of a 10-amino acid deletion in the putative tubulin-binding sequence of the C-terminus. This sequence only exists in GJA1 and is not

conserved in other gap junction protein families (Fig S2A) [30]. Microinjection of each dominant-negative mutant at ventral-animal regions of two-cell stage embryos caused severe defects in cilia formation (Fig 2A). Immunofluorescence analysis using an acetylated tubulin antibody showed severely shortened and fewer ciliary axonemes in the dnGJA1-injected embryos compared with those of control embryos (Fig 2A). In particular, the number of cilia on ciliated cells was notably decreased in Δ234–243 mutant-injected embryos, although it would be challenging to quantitatively analyze the phenotypes (Fig 2A). However, the basal bodies, which are the organizing center of ciliary axonemes, did not have noticeable defects, and the number of basal bodies and their apical localization were comparable to those of controls (Fig 2A, green). Next, we measured the number of ciliated cells by counting acetylated tubulin-positive cells, and indeed the number of ciliated cells was significantly reduced in the dnGJA1-expressing embryos (Fig 2B). We next isolated cilia from wild-type embryos or dnGJA1-injected embryos and analyzed the average length of isolated cilia. The ciliary length was significantly shorter in the dnGJA1 expressing embryos (Fig S2B, S2C).

Then, we examined localization of each dnGJA1 in multiciliated cells by expressing dnGJA-Flag mRNAs and observed that the Δ234–243 mutant did not exhibit ciliary axoneme localization, and the Δ130–136 mutant displayed reduced axonemal localization (Fig S2D). From these observations, we speculated that dnGJA1 may interfere with the proper localization of wild-type GJA1(wtGJA1) and thereby disrupt cilia formation. To test this idea, we co-injected HA-tagged wild-type GJA1 (wtGJA1-HA) and dnGJA1-Flag mRNA and analyzed the changes in wtGJA1-HA localization in multiciliated cells. As we speculated, co-injection of dnGJA1-Flag with wtGJA1-HA resulted in displacement of wtGJA1-HA from the ciliary axonemes (Fig 2C, 2D). These data suggest that the GJA1 function is necessary for proper cilia formation, especially ciliary axoneme assembly.

3. Morpholino-mediated knockdown of GJA1 disrupts normal ciliogenesis in *Xenopus.*

Next, we sought to further confirm the necessity of GJA1 in ciliogenesis by depleting proteins using an antisense morpholino oligo (GJA1-MO). To determine whether antisense MO-mediated knockdown of GJA1 also causes similar phenotypes to those of dominant-negative mutants, we designed an antisense MO to block translation by binding to the transcription start site. Antisense MO injection effectively reduced the translation of wild-type GJA1-Flag mRNA (Fig 3A). In contrast, the translation of mismatch GJA1 mRNA (mis-mGJA1), which was modified to be mismatched to the MO sequence, was not affected as strongly as that of wild-type mRNA (Fig 3A, MO+mis-mRNA). These data indicate that GJA1-MO specifically inhibits GJA1 mRNA translation.

We next analyzed the phenotype of GJA1-MO-injected embryos. Consistent with the mutant-based approaches, multiciliated cells in GJA1-MO-injected embryos (morphants) were severely malformed

compared to those of control embryos (Fig 3B), but basal bodies were not severely affected by GJA1-MO injection (Fig 3B, green). Moreover, MO-mediated knockdown of GJA1 resulted in a reduction of acetylated tubulin-positive multiciliated cells in *Xenopus* embryonic epithelial tissues (Fig 3C middle panel, 3E). Co-injection of MO-mismatched-GJA1 mRNA (mis-mGJA1) with GJA1-MO effectively rescued the ciliary defects (Fig 3C right panel, 3D, 3E), indicating that defects in cilia formation in GJA1 morphants are a specific loss-of-function phenotype of GJA1. We also co-injected each dnGJA1 mRNA with GJA1-MO. However, dominant-negative mutants failed to exhibit reversal of the ciliary defects seen in the GJA1 morphants (Fig 3D, 3E).

Based on the loss-of-function phenotype of GJA1 morphant embryos, we further determined whether GJA1 may affect cell fate specification during ciliated cell differentiation or whether it mainly affects ciliogenesis after cell fate determination. To this end, we performed whole-mount *in situ* hybridization using a DNAH9 antisense probe, which is a component of the ciliary outer dynein arm and is a known multiciliated cell marker [31]. In contrast to the reduction of acetylated tubulin-stained multiciliated cells in the embryonic epidermis of *Xenopus*, the number of DNAH9-positive multiciliated cells in GJA1 morphants was not significantly different from that in controls (Fig S3), which is implicating GJA1 did not affect the cell fate determination.

We further confirmed the GJA1 loss-of-function phenotype using CRISPR/Cas9-mediated F_0 mutagenesis by micro-injecting Cas9 and guide RNA (GJA1-Cas9) into two-cell stage embryos. Sequencing analysis and an *in vitro* Cas9 reaction using a PCR product covering the target site revealed that GJA1-Cas9 injection effectively induced indel mutations at the GJA1-Cas9 target sites (Fig S4A, S4B). Consistent with the GJA1 morphant phenotypes, we observed a reduction of acetylated tubulin-positive multiciliated cells (Fig S4C, S4D). These data indicate that GJA1 has previously unidentified but critical functions in cilia formation.

4. GJA1 function is necessary for gastrocoel roof plate cilium formation and left-right asymmetry development.

Motile cilia are not only involved in mucus clearance in the mucociliary epithelium but are also critical for determining left-right asymmetry during early embryonic development. Embryonic nodal cilium generates leftward flow, and this flow initiates the left lateral plate mesoderm (LPM) specification. In *Xenopus*, the gastrocoel roof plate (GRP) possesses a nodal cilium, and this mono-, motile nodal cilium is necessary for formation of left-right asymmetry [32, 33]. Therefore, we next determined whether GJA1 is also necessary for GRP cilium formation. GJA1-MO was injected into the two dorsal-vegetal cells in four-cell stage embryos to target GRP tissues. Indeed, GJA1 morphants displayed abnormally shortened nodal cilium in the GRP compared to those of control embryos (Fig

4A, 4B). Next, we assessed left-right asymmetry by observing heart development in later embryonic stages. In the ventral view, the truncus arteriosus of the control *Xenopus* embryonic heart was placed to the left of the embryos by looping of the primitive heart tube. We observed that approximately 30% of morphant embryos developed *situs inversus* (reversed organs) (Fig 4C, 4D supplementary video 1, 2). Furthermore, expression of the left LPM-specific marker PITX2 was abnormal in GJA1-morphant embryos (Fig 4E, 4F). These data demonstrate that GJA1 is also involved in motile nodal cilium formation in the GRP in *Xenopus.*

5. siRNA-mediated knockdown of GJA1 disrupts primary ciliogenesis in human RPE1 cells.

Because knockdown of GJA1 expression caused severe defects in the motile cilia of *Xenopus* epithelial tissues, we next examined the functions of GJA1 in primary ciliogenesis in human RPE cells. We first confirmed that low-serum starvation effectively initiated cilia formation in human RPE1 cells (Fig S5A, S5B). Then, we depleted GJA1 in human RPE1 cells by siRNA transfection, which was confirmed by immunoblotting (Fig S5C). Next, we observed primary cilium formation after inducing ciliogenesis under low-serum starvation conditions. Indeed, GJA1 depletion significantly disrupted cilia formation in RPE1 cells compared to control cells. Additionally, co-transfection of an siRNA-non-targetable-GJA1 cDNA plasmid with GJA1 siRNA partially rescued the siRNA phenotypes (Fig 5A, 5B). Next, we observed the localization of GJA1 in human RPE1 cells by performing an immunofluorescence analysis. As previously shown, GJA1 protein was localized to the gap junctions at the cell periphery (Fig 5A, yellow square). Unexpectedly, however, we did not observe ciliary localization of GJA1 in the primary cilium. GJA1 signals accumulated in pericentriolar regions, where the primary cilium originates (Fig 5C, white arrow). We further analyzed the subcellular localization of GJA1 by co-immunostaining GJA1 with the trans-Golgi marker TGN46 or the pericentriolar material (PCM) marker BBS4 and observed that GJA1 was broadly distributed in the Golgi and pericentriolar regions (Fig S6A). Interestingly, acetylated microtubules in the pericentriolar region were noticeably reduced in GJA1-depleted cells (Fig 5A) but the Golgi structure were not affected by GJA1 depletion (Fig S6B). From this observation, we speculated that GJA1 plays a role in primary cilium formation by affecting trafficking around the pericentriolar regions or PCM, which is involved in cilia formation [34].

Next, we examined the subcellular localization of several key proteins that are critical for ciliogenesis under GJA1-depleted conditions. Immunofluorescence staining of endogenous Arl13b, BBS4, CP110, IFT20, IFT88, and TTBK2, which are well-known PCM or ciliary markers (Fig S7A), was performed. BBS4 and CP110 showed abnormal distributions in GJA1 siRNA-transfected cells (Fig 6A-C), and no significant differences were found in the expression of other proteins, such as Arl13b, IFT20/88 and

TTBK2 (Fig S7B). During cell cycle progression, CP110 is localized at the cap of mother and daughter centrioles and inhibits ciliary axoneme elongation. For proper primary cilium formation, CP110 must be removed from the cap of the mother centriole to initiate elongation of the ciliary axonemes [35, 36]. In addition, BBS4, which is a component of the BBSome complex, is localized at the PCM and interacts with PCM-1, dynein, and intraflagellar transport protein (IFT) during the delivery of ciliary building blocks to ciliary axonemes (Fig S7A) [37, 38]. Interestingly, we frequently observed two CP110 spots in both mother and daughter centrioles in GJA1 siRNA-transfected RPE1 cells (Fig 6A, 6B). In addition, BBS4 was delocalized from the PCM and basal bodies (Fig 6C) with non-ciliogenesis phenotypes. Although the mechanism of CP110 during *Xenopus* multiciliogenesis has not been determined, CP110 phenotypes were similar to the GJA1 loss-of-function phenotype in RPE1 cells. GJA1-depleted embryos showed higher CP110 signal levels than those of wild-type embryos (Fig S8A, S8B). These data suggest that GJA1 is critical for primary cilium formation and may function in the cytoplasmic assembly of ciliogenesis factors around the pericentriolar region.

6. Rab11 interacts with GJA1, and knockdown of GJA1 interrupts Rab11 trafficking to basal bodies during ciliogenesis.

To identify the putative binding and functional partners of GJA1, we performed GJA1 IP-MS. Then, we performed Gene Ontology term analysis with 232 detected proteins and identified two major clusters of interest, regulation of Ca^{2+} and ciliogenesis (Fig S9, Table S1). A recent study revealed that gap junctions, especially those containing GJA1, mediate intracellular Ca^{2+} waves and regulate ependymal multicilia maintenance through the Wnt-GJA1-Ca^{2+} axis [20]. Therefore, we determined whether GJA1 depletion compromises cilia formation by affecting the intracellular Ca^{2+} concentration in RPE1 cells. GJA1 depletion or overexpression resulted in similar Ca^{2+} concentrations in the resting state and slightly affected Ca^{2+} entry compared with that in control RPE1 cells (Fig S10A, S10B). However, the difference in Ca^{2+} entry was not as significant as that in previously reported studies. Next, we focused on the clusters of ciliogenesis. Among dozens of interacting ciliary proteins, we selected Rab8a and Rab11a as candidates (Fig S9). Both Rab8 and Rab11 have previously been reported to be involved in ciliogenesis [25, 26, 38, 39]. Rab8 is localized in the primary cilium and regulates ciliary membrane extension [38, 39]. Previous studies have also shown that Rab8 interacts with CP110 and BBS4 [35, 36, 38]. Rab11 is enriched at the basal part of the primary cilium and recruits Rab8 to the basal body by interacting with Rabin8 [26, 39]. Additionally, during basal body maturation, Rab11-positive membrane vesicles are transported to the distal appendages of basal bodies and form large ciliary vesicles. This distal appendage vesicle assembly that forms ciliary vesicles is a prerequisite for CP110 removal and promotes the uncapping of the mother centrioles,

which is followed by the recruitment of intraflagellar transport proteins and transition zone proteins for ciliogenesis [40, 41].

We first confirmed the interaction between GJA1 and Rab8a or Rab11a by performing co-immunoprecipitation, followed by a western blot assay. Consistent with the IP-MS data, GJA1 was successfully immunoprecipitated with Rab8a (Fig S11A) or Rab11a (Fig 7A), whereas the rabbit IgG negative control did not show any signals. Next, we confirmed the localization of GJA1 and Rab11 during ciliogenesis. As expected, GJA1 and Rab11 were partially co-localized around the pericentriolar region and acetylated tubulin network (Fig 7B). In particular, GJA1 surrounded the Rab11 cluster, which was accumulated around the basal bodies. Furthermore, we observed decreased Rab8a and Rab11 protein levels in GJA1-depleted RPE1 cells (Fig S11B). Additionally, the accumulation of Rab11 at the base of the primary cilium was absent upon GJA1 depletion (Fig 7C-F). These phenotypes were partially rescued with GJA1-cloned plasmid co-transfected cells (Fig 7C, 7D). We further confirmed the presence of Rab11-positive ciliary vesicles using structured illumination microscopy (SIM). At higher resolutions, SIM analysis showed that Rab11-positive vesicles encircled the base of the ciliary axoneme. In contrast, GJA1-depleted cells showed scattered Rab11 signals (Fig 7E, 7F). We next investigated how dnGJA1 mutants may disturb ciliogenesis by performing co-immunoprecipitation with dnGJA1 proteins and Rab11a. Interestingly, all dnGJA1 mutant proteins failed to interact with Rab11a (Fig 8A, 8B)

Overall, these data suggest that GJA1 controls the trafficking of Rab11-positive vesicles to the base of cilia for ciliogenesis.

Discussion

The gap junction complex forms a channel that mediates cell-to-cell communication. Gap junction-mediated cell-to-cell communication is indispensable for normal embryonic development, and disruption of gap junction complex components causes embryonic lethality and various phenotypes in multiple organs [42-46]. For example, mutation of GJA1, which is a major gap junction complex component, causes a congenital disorder, ODDD, in humans [10]. Interestingly, recent studies have strongly suggested that GJA1 exerts diverse functions, in addition to gap junction formation, to control cellular migration and polarity via regulation of cytoskeleton components, such as actin filaments and microtubules, in various cell types, including cancer cells, neuronal progenitors, and cardiac neural crest cells [17, 19, 47, 48]. Additionally, the non-channel functions of GJA1 have been suggested to explain the complex disease phenotypes caused by GJA1 mutations in mice and humans

[45, 49, 50].

While we were examining the molecular mechanism of GJA1 in ciliogenesis, Zhang et al. published a paper arguing that GJA1 participates in the maintenance of ependymal motile cilia in the zebrafish spinal cord and in mouse models [20]. In this publication, Zhang et al. argued that GJA1 mediates the Ca^{2+} wave and signaling in the Wnt-PLC-IP3 cascade to maintain motile cilia.

In this study, we confirmed GJA1 localization around the pericentriolar region and ciliary axonemes for the first time, suggesting a direct function of GJA1 in ciliogenesis. Moreover, we confirmed that GJA1 depletion specifically affected CP110 removal from the mother centrioles and caused delocalization and BBS4-positive vesicle around the pericentriolar region; however, several other key ciliary and PCM molecules, such as Arl13b, IFT20, IFT88, and TTBK2, were not significantly affected. These data suggest that GJA1 may perform specific functions in general ciliogenesis, in addition to functioning as a mediator of the Ca^{2+} wave, for the maintenance of motile cilia.

Furthermore, in IP-MS assays, we found that Rab11 interacted with GJA1, which can explain how GJA1 controls CP110 removal from the mother centriole for ciliogenesis. Rab11 is a major regulator of ciliary vesicle trafficking and is necessary for ciliary vesicle accumulation on the mother centriole, which is suggested to be a prerequisite for removal of CP110 from the mother centriole [40, 41]. Finally, we showed that the dnGJA1 mutant proteins in this study failed to interact with Rab11a, which may explain how GJA1 controls cilia formation. Our findings strongly support that GJA1 controls trafficking and accumulation to Rab11/8 positive vesicles in the mother centriole and hence facilitates removal of CP110 to initiate cilia formation and this process is probably necessary pericentriolar microtubule networks (Fig 8C).

Previous studies have investigated the possible function of gap junction proteins, such as GJB2 (gap junction protein β2; CX26), GJA1 (CX43), and GJA7 (gap junction protein α7; CX43.4), in determining left-right asymmetry. Most studies on the function of gap junction proteins in determining laterality have indicated that the channel function is critical for mediating leftward signals, which are driven by nodal cilia [51-53]. For example, GJB2 is a key gap junction protein involved in determining left-right asymmetry, whereas the GRP cilium is largely unaffected by GJB2 depletion [51].

Our study supports that GJA1, a major connexin (CX43), is critical for formation of both motile and primary cilia. The cytosolic domain of GJA1 contains a microtubule-binding motif that is necessary for trafficking to the gap junction complex. Furthermore, GJA1 seems to exhibit gap junction-independent functions that mainly control the cytoskeleton and provide directional cues for migrating cells [30, 47, 54]. Interestingly, cilia have also been shown to be necessary for the polarization of migrating cells and directional protrusions, such as lamellipodia [55, 56]. Given the complex loss-of-

function phenotype of GJA1, it is feasible to hypothesize that some gap-junction-independent functions of GJA1 may be mediated by regulating cilia formation. GJA1 was localized around the pericentriolar region in human RPE1 cells, and GJA1 depletion resulted in reduced acetylated tubulin levels in pericentriolar microtubules. Pericentriolar microtubules are critical for the transport of ciliary building blocks and are involved in cilia formation by organizing ciliary protein transport [57-59]. Further studies to examine the molecular functions of GJA1 in transporting ciliary building blocks may elucidate the molecular function of GJA1 in cilia formation.

Materials and Methods

1. *Xenopus laevis* rearing

Adult female and male *Xenopus laevis* were provided by the Korea National Research Resource Center (KNRRC, KXRCR000001, KXRCR000002). Ovulation was induced in adult female *Xenopus laevis* by injection of human chorionic gonadotropin. Eggs were then fertilized *in vitro* and dejellied with 3% cysteine in 1/3× Marc's Modified Ringers (MMR) (pH 7.8–7.9) solution. After fertilization, eggs were reared in 1/3× MMR solution.

1.1. Microinjection procedure

For microinjections, embryos were placed in 1% Ficoll in 1/3× MMR solution. To target the epithelial or GRP tissue in *Xenopus* embryos, we injected into the ventral-animal region (epithelial tissue) or dorsal-vegetal region (GRP tissue) of blastomeres in the two- or four-cell stage [60] using a Picospritzer III microinjector (Parker, NH, USA). The injected eggs were grown in 1/3× MMR with an antibiotic (gentamycin). We injected 80 ng of MO per embryo, and wild-type or dominant-negative mutant mRNAs were injected in various amounts.

1.2. Morpholino

We designed a translation-blocking antisense MO for GJA1 based on the sequence from the Xenbase database. The MO was manufactured by Gene Tools (OR, USA) (GJA1-MO: 5'-TTCCTAAGGCACTCCAGTCACCCAT-3').

1.3. Fixation

To analyze epithelial cilia development, we fixed embryos at stage 26–30 using MEMFA (2× MEM salts and 7.5% formaldehyde) or Dent's fixative solution (20% DMSO in methanol).

1.4. Cilia isolation

Cilia isolation was performed using a modified Ca^{2+} shock method, as previously described [61], Briefly, deciliation solution (20 mM Tris-HCl [pH 7.5], 50 mM NaCl, 10 mM $CaCl_2$, 1 mM EDTA, 7 mM β-mercaptoethanol, and 0.1% Triton X-100) was added to the embryos, and the test tube was gently inverted for 30 seconds. To remove the cellular debris, samples were centrifuged at 1500 g for 2 min, and the supernatants were transferred to new e-tubes. Cilia in the supernatant were pelleted by centrifugation at 12,000 g for 5 min. After discarding the supernatant, MEMFA or Dent's fixative solution was added immediately to fix the cilia pellet.

1.5. *In situ* hybridization

Whole-mount *in situ* hybridization was performed with a modified method, as previously described [62]. The antisense probe was transcribed from the approximately 800 bp amplified PCR product of PITX2 (Primer; Sense: 5'-CGCAAACTGGTGACAACCTGTG-3', SP6-antisense: 5'-gcgatttaggtgacactatagTGCCAGGCTGGAGTTACATGTG-3') or DNAH9 (Primer; Sense: 5'-ACAGGCTGGTGCTGCAGGA-3', SP6-antisense: 5'-gcgatttaggtgacactatagCAAAATGACGCTGGAGGGG-3') using the mMESSAGE mMACHINE™ SP6 Transcription Kit (Invitrogen, ThermoFisher Scientific, MA, USA) and a dig-dNTP mix (Roche, Basel, Switzerland).

1.6. GRP tissue explant preparation

GRP tissue explants were prepared as previously described [33]. To image GRP nodal cilium, stage 17 embryos were fixed and sliced at the anterior head before immunofluorescence staining. Then, GRP tissue explants were mounted on a cover glass.

1.7. Genome editing with CRISPR/Cas9 technology

The *Xenopus laevis* GJA1 crRNA sequence was designed using the CHOPCHOP website. The designed GJA1 crRNA (Sense: 5'-GTCTGCAATACTCAGCAACCagg-3') and Alt-R® CRISPR-Cas9 crRNA and the tracrRNAs were purchased from IDT. GJA1 CRISPR/Cas9 was prepared using

the protocol provided by the manufacturer. spCas9 protein with guide RNA (RNP) was injected into the ventral-animal region of the blastomeres at the two-cell stage. We injected 20 fmol RNP in each embryo. Genomic DNA was extracted from stage 28 embryos to confirm GJA1 CRISPR/Cas9 efficiency. Genomic DNA was used in PCR amplification with specific primer pairs, which targeted the vicinity of the guide RNA sequence. The amplified PCR product was used for *in vitro* CRISPR/Cas9 experiments or sequencing analysis (Bionics, Seoul, Republic of Korea).

2. Human RPE1 cell culture

Human RPE1 cells were obtained from ATCC (VA, USA, CRL-4000™) and were cultured under standard mammalian cell conditions with 10% FBS (Gibco, ThermoFisher Scientific) and 1% antibiotics in DMEM/F12 (1:1) media (Gibco).

2.1. Transfection

For GJA1 siRNA knockdown experiments, RPE1 cells were transfected with siRNA (Genolution, Seoul, Republic of Korea, sense, 5'-GUUCAAGUACGGUAUUGAAUU-3') using jetPRIME® transfection reagent (Polyplus, NY, USA). Exogenous plasmid DNA was transfected using Transporter™ 5 transfection reagent (Polysciences, PA, USA). Co-transfection of siRNA with plasmid DNA was performed using jetPRIME® transfection reagent. All transfections were performed in Opti-MEM® medium (Gibco). The final concentration of siRNA was 70 nM. Transfected cells were incubated for 48 hours, including the serum starvation step.

2.2. Ciliation and serum starvation

For primary ciliation of RPE1 cells, the cells were incubated in serum-free DMEM/F12 medium (Gibco) for at least 24 hours.

2.3. Fixation

To analyze primary cilium development, RPE1 cells were fixed in PFA (4% formaldehyde in 1× PBS) fixative solution after ciliation.

2.4. Intracellular Ca^{2+} entry imaging

For intracellular Ca^{2+} imaging, GJA1 siRNA- or plasmid DNA-transfected RPE1 cells were cultured on fibronectin (Sigma Aldrich, MO, USA)-coated cover glasses. Cells were loaded with 2 μM Fura-2/AM (Invitrogen). Ratiometric Ca^{2+} imaging was performed at 340 and 380 nm in 0 or 2 mM Ca^{2+} Ringer's solution using an IX81 microscope (Olympus, Tokyo, Japan) at room temperature. Images were processed with Metamorph and analyzed with Igor Pro software. Ca^{2+} peaks were calculated by determining the maximum of each trace upon application of 0.5 μM thapsigargin (Santa Cruz, TX, USA) and Ca^{2+}, and baseline values before application were subtracted.

3. Mouse trachea isolation, vibratome sectioning, and imaging preparation

Mouse tracheal tissues were isolated from wild-type mice. Isolated tracheal tissues were fixed with 4% PFA for 1 hour at room temperature with mild shaking and mounted in 3% low-melting point agarose gel (BioShop, Ontario, Canada) in 1× PBS. Mounted tracheal tissues were sectioned into 100 μm slices with a vibratome (VT1000 S, Leica). Sectioned samples were immunostained and mounted with BA:BB solution (both from Sigma Aldrich) for tissue clearing.

4. Cloning and plasmid information

The full-length sequences of the *Xenopus laevis* GJA1 and human GJA1, Rab8a, and Rab11a genes were obtained from the Xenbase database or PubMed. Total *Xenopus laevis* RNA was purified from stage 35–36 embryos, and total human RNA was purified from RPE1 cells. Next, we reverse-transcribed cDNA with a random primer mix (NEB, MA, USA) and GoScript™ Reverse Transcriptase (Promega, WI, USA). We designed the primer pairs with a restriction enzyme site for cloning (Table 1). For the rescue experiments, point mutations were generated in the MO- or siRNA-binding sequences of GJA1 cDNA. We designed the primer pairs to generate a silencing point mutation (Table 1). Amplified *Xenopus* GJA1 and human GJA1, Rab8a, and Rab11a PCR products were cloned into the CS108 or pcDNA3.0 vectors and fused to Flag- or HA-tag sequences at the C-terminus of the coding sequence. Dominant-negative forms of GJA1 constructs were generated based on the cloned *Xenopus laevis* wild-type GJA1-Flag plasmid with deletion or point mutation primer pairs (Table 1). After PCR amplification using the primers, the DpnI enzyme was added, and the PCR product was transformed into DH5α *E. coli*. Wild-type or dominant-negative GJA1 mRNAs were transcribed from the cloned plasmid using an mMESSAGE mMACHINE™ SP6 Transcription Kit (Invitrogen).

Table 1. Primer information

Primer Name	Primer Sequences (5' – 3')
SalI-xlGJA1-Forward	aatgtcgacATGGGTGACTGGAGTGCCTTAGG
XbaI-xlGJA1-Backward	aattctagaGATCTCTAAATCATCAGGTCGTGGTCT
SalI-hGJA1-Forward	aatgtcgacATGGGTGACTGGAGCGCCT
XbaI-hGJA1-Backward	aattctagaGATCTCCAGGTCATCAGGCCG
point mut-xlGJA1-Forward	CGACATGGGGGATTGGAGCGCATTGGGAAGACTT
point mut-xlGJA1-Backward	AGTCTTCCCAATGCGCTCCAATCCCCCATGTCGA
point mut-hGJA1-Forward	TGAGATAAAGAAATTTAAATATGGAATAGAGGAGCATGGT AAGGTGAAA
point mut-hGJA1-Backward	CTTACCATGCTCCTCTATTCCATATTTAAATTTCTTTATCTC AATCTGC
SalI-hRab8a-Forward	aatgtcgacATGGCGAAGACCTACGATTACCTG
XbaI-hRab8a-Backward	aattctagaCAGAAGAACACATCGGAAAAAGCTG
SalI-hRab11a-Forward	aatgtcgacATGGGCACCCGCGACG
XbaI-hRab11a-Backward	aattctagaGATGTTCTGACAGCACTGCACCTT
xlGJA1-T154A-Forward	AAAGTCAAGATGCGAGGTGGACTGCTTCGCGCCTACATC ATCAGCATTTTGTTTAAA
xlGJA1-T154A-Backward	TACTGATTTAAACAAAATGCTGATGATGTAGGCGCGAAGC AGTCCACCTCGCATCTT
xlGJA1-Δ130–136-Forward	ATGCACCTTAAACAATATGGCCTTGAAGAG
xlGJA1-Δ130–136-Backward	CTCTTCAAGGCCATATTGTTTAAGGTGCAT
xlGJA1-Δ234–243-Forward	TTCTATGTCACCTACAAAGACCCATTTTCT
xlGJA1-Δ234–243-Backward	AGAAAATGGGTCTTTGTAGGTGACATAGAA

5. Immunofluorescence

Embryos were fixed with MEMFA or Dent's fixative solution overnight at 4°C, and RPE1 cells were fixed with 4% PFA solution for 20 min at room temperature. Fixed embryos or RPE1 cells were incubated in a blocking solution (10% FBS and 2% DMSO in 1× TBS with 0.1% Triton X-100) for 30 min at room temperature to block non-specific binding. Immunostaining was performed with the following antibodies at 1:50–500 dilutions in blocking solution for 1–2 hours at room temperature: anti-DDDD-K (Abcam, Cambridge, UK, ab1162), anti-GFP (ThermoFisher Scientific, A10262), anti-HA (Santa Cruz, sc-7392), anti-RFP (Abcam, ab62341), anti-acetylated tubulin (Sigma Aldrich, T7451), anti-γ-tubulin (Abcam, ab191114), anti-MyHC (DSHB, IA, USA, A4.1025), anti-CP110 (Proteintech, IL, USA, 12780-1-AP), anti-BBS4 (Proteintech, 12766-1-AP), anti-TGN46 (Abcam, ab50595), anti-Arl13b (Proteintech, 17711-1-AP), anti-TTBK2 (Proteintech, 15072-1-AP), anti-IFT20 (Proteintech, 13615-1-AP), anti-IFT88 (Proteintech, 13967-1-AP), anti-Rab8a (CST, MA, USA, #6975), anti-Rab11 (CST, #5589), and anti-GJA1 (both ThermoFisher Scientific, PA1-25098, 13-8300). Fluorescence labeling was performed using DAPI (1:10,000, ThermoFisher Scientific, D1306), and Alexa Fluor 488-, 555-, and 633-conjugated secondary antibodies (1:300, All ThermoFisher Scientific).

6. Immunoblotting

Xenopus or human RPE1 immunoblotting samples were prepared with modified lysis buffer (TBS, 1% Triton X-100, and 10% glycerol with protease inhibitor). After removing fat and cellular debris, a sodium dodecyl sulfate (SDS) sample buffer with dithiothreitol (DTT) was added. Samples were loaded on SDS-polyacrylamide gels and transferred to polyvinylidene fluoride membranes (Merck Millipore, MA, USA). Membranes were incubated in blocking solution (TBS, 0.05% Tween-20 with non-fat powdered milk) for 30 min at room temperature to block non-specific binding. Immunoblotting was performed with the following antibodies at 1:2,500–3,000 dilutions for either 1 hour at room temperature or overnight at 4°C: anti-DDDD-K (Abcam, ab1162), anti-α-actin (ThermoFisher Scientific, MA1-744), anti-α-tubulin (Abcam, ab15246), anti-GJA1 (ThermoFisher Scientific, PA1-25098), anti-HA (Santa Cruz, sc-7392), anti-Rab8a (CST, #6975), and anti-Rab11 (CST, #5589). Secondary labeling was performed using horseradish peroxidase-conjugated anti-mouse or anti-rabbit IgG antibodies (1:3,000, both ThermoFisher Scientific, 31430, 31460) for 1 hour at room temperature. Chemiluminescence was performed with SuperSignal™ West Dura Extended Duration Substrate (ThermoFisher Scientific, 34076), and the membranes were imaged with an iBright imaging system (FL1000, ThermoFisher Scientific).

7. Immunoprecipitation and mass spectrometry

For immunoprecipitation of GJA1, we produced anti-GJA1 antibody-conjugated paramagnetic beads. Anti-GJA1 antibody (ThermoFisher Scientific) or normal rabbit serum (Abclon, Seoul, Republic of Korea) was cross-linked with Protein G Mag Sepharose beads (GE Healthcare, IL, USA), according to the manufacturer's instructions. Human RPE1 lysate was prepared with immunoblotting lysis buffer and incubated with GJA1- or rabbit serum-conjugated beads overnight at 4°C. The beads were washed with lysis buffer and eluted with low-pH elution buffer (0.1 M glycine-HCl, pH 2.9). Next, eluted samples were concentrated using Amicon® Ultra (Merck Millipore), and SDS sample buffer and DTT were added. For mass spectrometry, protein samples were separated on a 12% Tris-glycine SDS-polyacrylamide gel. The gel was stained with Coomassie brilliant blue G-250 overnight, after which it was destained with a destaining solution (10% ethanol/2% orthophosphoric acid). Gel pieces were destained in 1:1 methanol:50 mM ammonium bicarbonate, and destained gels were dehydrated with 100% acetonitrile and then incubated in 25 mM DTT in 50 mM ammonium bicarbonate for 20 min at 56°C. After removing the DTT solution, the samples were alkylated in 25 mM iodoacetamide in 100 mM ammonium bicarbonate solution. The iodoacetamide solution was removed, and then the samples were dehydrated with 100% acetonitrile. Approximately 0.25 μg of mass-spectrometry-grade trypsin protease was added to each sample, along with 100 μL of a 50 mM ammonium bicarbonate/10%

acetonitrile solution. Protein samples were then digested overnight at 37°C. After digestion, 100 μL of 50% acetonitrile/0.1% formic acid solution was added to the trypsin solution for 3 min at 56°C. Extraction solution (99.9% acetonitrile/0.1% formic acid; 100 μL) was added to each sample for 3 min at 56°. Collected peptides were dried and dissolved with 20 μL of 0.1% Trifluoroacetic acid solution and purified with C18 tips. Eluted samples were dried completely in a vacuum concentrator and resuspended with 20 μL of 0.1% formic acid solution. The samples were analyzed with a high-resolution mass spectrometer (Orbitrap Fusion Lumos, ThermoFisher Scientific). Immunoprecipitation analysis of the GJA1 and Rab proteins was performed using anti-GJA1 antibody-conjugated beads, which were described above, and wild-type or dominant-negative GJA1 and Rab11a mutants were detected using anti-Flag M2 magnetic beads (Sigma Aldrich), which captured the GJA1 Flag-tagged proteins, using an equal lysis and immunoprecipitation method. The raw data of GJA1 IP/MS analysis were uploaded to the Dryad (https://datadryad.org/stash/share/2vr1tLjIBBIikUC9q9jNaxAi0Rl7Us9tGwByO4HyodU, Table S1).

8. Microscopy, image analysis and Statistical analysis

Images were captured by confocal microscopy (LSM780, LSM880, both from Zeiss, Oberkochen, Germany), stereo microscopy (SZX16, Olympus), and SIM (ELYRA S.1, Zeiss). Image analyses were performed using ZEN software for merging, 3D images, and SIM processing. For the randomization of statistical analysis, the images were randomly taken from the samples and individual cells in the wide field of image were analyzed. Quantitative analyses of the average ciliary length and number of multiciliated or RPE1 cells were performed with the ZEN and ImageJ programs. Statistical analysis including error bars with mean±s.d. and P values was calculated using a two-tailed t-test, one-way ANOVA, or two-way ANOVA using Prism 9.

9. Animal ethics

All animal experiments were performed with appropriate ethical approval from the UNIST Institutional Animal Care and Use Committee (UNISTIACUC-19-22, UNISTIACUC-20-26).

10. materials availability

All materials newly created in this work are available upon request.

Acknowledgments

The authors thank Dr. M. Ko and Dr. S. H. Park for critical discussions.

This work was supported by the Korea National Research Foundation (2021R1A2B5B02002285) and Institute for Basic Science (IBS-R001-D1).

Competing interests

The authors declare no competing interests.

References

1. Goodenough, D.A., J.A. Goliger, and D.L. Paul, *Connexins, connexons, and intercellular communication.* Annu Rev Biochem, 1996. **65**: p. 475-502.
2. Goodenough, D.A. and D.L. Paul, *Gap junctions.* Cold Spring Harb Perspect Biol, 2009. **1**(1): p. a002576.
3. Aasen, T., *Connexins: junctional and non-junctional modulators of proliferation.* Cell Tissue Res, 2015. **360**(3): p. 685-99.
4. El-Sabban, M.E., L.F. Abi-Mosleh, and R.S. Talhouk, *Developmental regulation of gap junctions and their role in mammary epithelial cell differentiation.* J Mammary Gland Biol Neoplasia, 2003. **8**(4): p. 463-73.
5. Vinken, M., et al., *Connexins and their channels in cell growth and cell death.* Cell Signal, 2006. **18**(5): p. 592-600.
6. Bosco, D., J.A. Haefliger, and P. Meda, *Connexins: key mediators of endocrine function.* Physiol Rev, 2011. **91**(4): p. 1393-445.
7. Söhl, G. and K. Willecke, *Gap junctions and the connexin protein family.* Cardiovasc Res, 2004. **62**(2): p. 228-32.
8. Beyer, E.C., D.L. Paul, and D.A. Goodenough, *Connexin43: a protein from rat heart homologous to a gap junction protein from liver.* J Cell Biol, 1987. **105**(6 Pt 1): p. 2621-9.
9. Boyadjiev, S.A., et al., *Linkage analysis narrows the critical region for oculodentodigital dysplasia to chromosome 6q22-q23.* Genomics, 1999. **58**(1): p. 34-40.
10. Paznekas, W.A., et al., *Connexin 43 (GJA1) mutations cause the pleiotropic phenotype of oculodentodigital dysplasia.* Am J Hum Genet, 2003. **72**(2): p. 408-18.
11. Oyamada, M., Y. Oyamada, and T. Takamatsu, *Regulation of connexin expression.* Biochim Biophys Acta, 2005. **1719**(1-2): p. 6-23.

12. Evans, W.H. and P.E. Martin, *Gap junctions: structure and function (Review).* Mol Membr Biol, 2002. **19**(2): p. 121-36.
13. Ruangvoravat, C.P. and C.W. Lo, *Connexin 43 expression in the mouse embryo: localization of transcripts within developmentally significant domains.* Dev Dyn, 1992. **194**(4): p. 261-81.
14. Willecke, K., et al., *Structural and functional diversity of connexin genes in the mouse and human genome.* Biol Chem, 2002. **383**(5): p. 725-37.
15. Beyer, E.C., D.L. Paul, and D.A. Goodenough, *Connexin family of gap junction proteins.* J Membr Biol, 1990. **116**(3): p. 187-94.
16. Leithe, E., M. Mesnil, and T. Aasen, *The connexin 43 C-terminus: A tail of many tales.* Biochim Biophys Acta, 2018. **1860**(1): p. 48-64.
17. Matsuuchi, L. and C.C. Naus, *Gap junction proteins on the move: connexins, the cytoskeleton and migration.* Biochim Biophys Acta, 2013. **1828**(1): p. 94-108.
18. Kameritsch, P., K. Pogoda, and U. Pohl, *Channel-independent influence of connexin 43 on cell migration.* Biochim Biophys Acta, 2012. **1818**(8): p. 1993-2001.
19. Rhee, D.Y., et al., *Connexin 43 regulates epicardial cell polarity and migration in coronary vascular development.* Development, 2009. **136**(18): p. 3185-93.
20. Zhang, J., et al., *Wnt-PLC-IP3-Connexin-Ca(2+) axis maintains ependymal motile cilia in zebrafish spinal cord.* Nat Commun, 2020. **11**(1): p. 1860.
21. Gerdes, J.M., E.E. Davis, and N. Katsanis, *The vertebrate primary cilium in development, homeostasis, and disease.* Cell, 2009. **137**(1): p. 32-45.
22. Malicki, J.J. and C.A. Johnson, *The Cilium: Cellular Antenna and Central Processing Unit.* Trends Cell Biol, 2017. **27**(2): p. 126-140.
23. Waters, A.M. and P.L. Beales, *Ciliopathies: an expanding disease spectrum.* Pediatr Nephrol, 2011. **26**(7): p. 1039-56.
24. Fliegauf, M., T. Benzing, and H. Omran, *When cilia go bad: cilia defects and ciliopathies.* Nat Rev Mol Cell Biol, 2007. **8**(11): p. 880-93.
25. Knodler, A., et al., *Coordination of Rab8 and Rab11 in primary ciliogenesis.* Proc Natl Acad Sci U S A, 2010. **107**(14): p. 6346-51.
26. Westlake, C.J., et al., *Primary cilia membrane assembly is initiated by Rab11 and transport protein particle II (TRAPPII) complex-dependent trafficking of Rabin8 to the centrosome.* Proc Natl Acad Sci U S A, 2011. **108**(7): p. 2759-64.
27. James-Zorn, C., et al., *Xenbase: expansion and updates of the Xenopus model organism database.* Nucleic Acids Res, 2013. **41**(Database issue): p. D865-70.
28. Beahm, D.L., et al., *Mutation of a conserved threonine in the third transmembrane helix of alpha- and beta-connexins creates a dominant-negative closed gap junction channel.* J Biol Chem, 2006. **281**(12): p. 7994-8009.

29. Wang, M., et al., *Connexin43 with a cytoplasmic loop deletion inhibits the function of several connexins.* Biochem Biophys Res Commun, 2005. **333**(4): p. 1185-93.
30. Giepmans, B.N., et al., *Gap junction protein connexin-43 interacts directly with microtubules.* Curr Biol, 2001. **11**(17): p. 1364-8.
31. Fassad, M.R., et al., *Mutations in Outer Dynein Arm Heavy Chain DNAH9 Cause Motile Cilia Defects and Situs Inversus.* Am J Hum Genet, 2018. **103**(6): p. 984-994.
32. Schweickert, A., et al., *Cilia-driven leftward flow determines laterality in Xenopus.* Curr Biol, 2007. **17**(1): p. 60-6.
33. Blum, M., et al., *Xenopus, an ideal model system to study vertebrate left-right asymmetry.* Dev Dyn, 2009. **238**(6): p. 1215-25.
34. Moser, J.J., et al., *The PCM-basal body/primary cilium coalition.* Semin Cell Dev Biol, 2010. **21**(2): p. 148-55.
35. Tsang, W.Y., et al., *CP110 suppresses primary cilia formation through its interaction with CEP290, a protein deficient in human ciliary disease.* Dev Cell, 2008. **15**(2): p. 187-97.
36. Tsang, W.Y. and B.D. Dynlacht, *CP110 and its network of partners coordinately regulate cilia assembly.* Cilia, 2013. **2**(1): p. 9.
37. Uytingco, C.R., et al., *BBS4 is required for intraflagellar transport coordination and basal body number in mammalian olfactory cilia.* J Cell Sci, 2019. **132**(5).
38. Nachury, M.V., et al., *A core complex of BBS proteins cooperates with the GTPase Rab8 to promote ciliary membrane biogenesis.* Cell, 2007. **129**(6): p. 1201-13.
39. Blacque, O.E., N. Scheidel, and S. Kuhns, *Rab GTPases in cilium formation and function.* Small GTPases, 2018. **9**(1-2): p. 76-94.
40. Sanchez, I. and B.D. Dynlacht, *Cilium assembly and disassembly.* Nat Cell Biol, 2016. **18**(7): p. 711-7.
41. Lu, Q., et al., *Early steps in primary cilium assembly require EHD1/EHD3-dependent ciliary vesicle formation.* Nat Cell Biol, 2015. **17**(3): p. 228-240.
42. Meşe, G., G. Richard, and T.W. White, *Gap junctions: basic structure and function.* J Invest Dermatol, 2007. **127**(11): p. 2516-24.
43. Laird, D.W., *The gap junction proteome and its relationship to disease.* Trends Cell Biol, 2010. **20**(2): p. 92-101.
44. Dobrowolski, R. and K. Willecke, *Connexin-caused genetic diseases and corresponding mouse models.* Antioxid Redox Signal, 2009. **11**(2): p. 283-95.
45. Pfenniger, A., A. Wohlwend, and B.R. Kwak, *Mutations in connexin genes and disease.* Eur J Clin Invest, 2011. **41**(1): p. 103-16.
46. Srinivas, M., V.K. Verselis, and T.W. White, *Human diseases associated with connexin mutations.* Biochim Biophys Acta Biomembr, 2018. **1860**(1): p. 192-201.

47. Francis, R., et al., *Connexin43 modulates cell polarity and directional cell migration by regulating microtubule dynamics.* PLoS One, 2011. **6**(10): p. e26379.

48. Crespin, S., et al., *The carboxy-terminal tail of connexin43 gap junction protein is sufficient to mediate cytoskeleton changes in human glioma cells.* J Cell Biochem, 2010. **110**(3): p. 589-97.

49. Laird, D.W., *Syndromic and non-syndromic disease-linked Cx43 mutations.* FEBS Lett, 2014. **588**(8): p. 1339-48.

50. Laird, D.W., *Closing the gap on autosomal dominant connexin-26 and connexin-43 mutants linked to human disease.* J Biol Chem, 2008. **283**(6): p. 2997-3001.

51. Beyer, T., et al., *Connexin26-mediated transfer of laterality cues in Xenopus.* Biol Open, 2012. **1**(5): p. 473-81.

52. Levin, M. and M. Mercola, *Gap junctions are involved in the early generation of left-right asymmetry.* Dev Biol, 1998. **203**(1): p. 90-105.

53. Hatler, J.M., J.J. Essner, and R.G. Johnson, *A gap junction connexin is required in the vertebrate left-right organizer.* Dev Biol, 2009. **336**(2): p. 183-91.

54. Fu, Y., et al., *Cx43 Isoform GJA1-20k Promotes Microtubule Dependent Mitochondrial Transport.* Front Physiol, 2017. **8**: p. 905.

55. Veland, I.R., L. Lindbaek, and S.T. Christensen, *Linking the Primary Cilium to Cell Migration in Tissue Repair and Brain Development.* Bioscience, 2014. **64**(12): p. 1115-1125.

56. Schneider, L., et al., *Directional cell migration and chemotaxis in wound healing response to PDGF-AA are coordinated by the primary cilium in fibroblasts.* Cell Physiol Biochem, 2010. **25**(2-3): p. 279-92.

57. Kim, J., S.R. Krishnaswami, and J.G. Gleeson, *CEP290 interacts with the centriolar satellite component PCM-1 and is required for Rab8 localization to the primary cilium.* Hum Mol Genet, 2008. **17**(23): p. 3796-805.

58. Kim, K., K. Lee, and K. Rhee, *CEP90 is required for the assembly and centrosomal accumulation of centriolar satellites, which is essential for primary cilia formation.* PLoS One, 2012. **7**(10): p. e48196.

59. Lopes, C.A., et al., *Centriolar satellites are assembly points for proteins implicated in human ciliopathies, including oral-facial-digital syndrome 1.* J Cell Sci, 2011. **124**(Pt 4): p. 600-12.

60. Hubrecht-Laboratorium (Embryologisch Instituut), P.D. Nieuwkoop, and J. Faber, *Normal table of Xenopus laevis (Daudin). A systematical and chronological survey of the development from the fertilized egg till the end of metamorphosis.* 2. ed. 1967, Amsterdam,: North-Holland Pub. Co. 260 p. with illus. with 10 fold. l.

61. Hastie, A.T., et al., *Isolation of cilia from porcine tracheal epithelium and extraction of dynein arms.* Cell Motil Cytoskeleton, 1986. **6**(1): p. 25-34.

62. Harland, R.M., *In situ hybridization: an improved whole-mount method for Xenopus embryos.* Methods Cell Biol, 1991. **36**: p. 685-95.

Figure legends

Figure 1. GJA1 is localized at the ciliary base and axonemes in addition to gap junctions in *Xenopus* multiciliated epithelial cells.

A. The schematic structure of gap junction channels and GJA1.

B, C. Immunofluorescence analysis of the localization of GJA1 in *Xenopus* multiciliated epithelial cells. *Xenopus* embryos were microinjected with GJA1-Flag mRNA, and the embryos were stained with antibodies against acetylated tubulin (red) and Flag-tag (green). Scale bars: 10 µm

D. Immunofluorescence analysis of the localization of GJA1 and the basal body marker centrin in *Xenopus* multiciliated epithelial cells. *Xenopus* embryos were co-microinjected with GJA1-HA mRNA and centrin-GFP mRNA. The embryos were stained with antibodies against HA-tag (green) and GFP (red). Scale bars: 10 µm

B'–D'. X-Z projection images of panels **B–D.**

Figure 2. GJA1 dysfunction causes ciliary defects in *Xenopus* multiciliated epithelial cells.

A. *Xenopus* embryos were injected with the indicated dnGJA1 mRNAs, and the mucociliary epithelium was immunostained. The ciliary axonemes were stained with acetylated tubulin antibody (red). Basal bodies were visualized by microinjection of centrin-GFP (green). Plasma membranes were labeled with membrane RFP and detected using an anti-RFP antibody (blue). Scale bars: 10 µm.

B. Statistical analysis of the number of multiciliated cells per unit area in panel **(A)**. Error bars represent the mean±s.d. P values were determined by one-way ANOVA (P****<0.0001). Raw values are provided in the source data file.

C. *Xenopus* laevis embryos were co-microinjected with HA-tagged wild-type GJA1 (wtGJA1-HA) and Flag-tagged dominant-negative mutant GJA1 (dnGJA1-Flag) mRNAs. Wild-type GJA1 was stained with an HA antibody (green), and each dominant-negative mutant GJA1 was stained with a Flag antibody (red). Scale bars: 10 µm.

D. Statistical analysis of GJA1 intensity as a ratio of that in the ciliary axoneme to that in the cytoplasm in panel **(C)**. Error bars represent the mean±s.d. P values were determined by one-way ANOVA ($P^{****}<0.0001$, $P^{*}=0.0194$). Raw values are provided in the source data file.

Figure 3. Morpholino-mediated knockdown of GJA1 causes severe disruption of ciliogenesis in *Xenopus* multiciliated epithelial cells.

A. Wild-type GJA1 (Wt-GJA1-Flag) mRNA or silent mutant mRNA (Mis-mGJA1-Flag; non-targetable by GJA1-MO), which was modified to be mismatched to the MO sequence, was co-injected with GJA1-MO into embryos. Immunoblotting was performed with an anti-Flag antibody for GJA1-Flag or with α-tubulin as the loading control. GJA1-MO efficiently inhibited GJA1-Flag expression from Wt-GJA1 mRNA.

B. Microinjection of a GJA1 antisense morpholino (GJA1-MO) disrupted normal ciliary axoneme assembly in multiciliated cells. The ciliary axonemes were labeled with an acetylated tubulin antibody (red), and centrosomes or basal bodies were stained with a γ-tubulin antibody (green). The cell membranes were labeled by microinjection of membrane RFP and detected using an anti-RFP antibody (blue). Scale bars: 10 µm.

C. Low-magnification confocal images of *Xenopus* multiciliated epithelial cells. Embryos were either injected with GJA1-MO alone or co-injected with MO-mismatched-GJA1 mRNA (Mis-mGJA1) and GJA1-MO. Mis-mGJA1 mRNA effectively rescued the ciliary defects. Multi-cilia bundles were stained with acetylated tubulin (red), and membranes were labeled by microinjection of membrane-GFP and detected with an anti-GFP antibody (green). Scale bars: 100 µm.

D. Flag-tagged wild-type or dominant-negative GJA1 mutant mRNAs were co-injected with GJA1-MO. All mutant mRNAs contained MO-mismatched target sequences. Only WT-GJA1-Flag mRNA rescued the loss-of-function phenotype. Each GJA1 Flag-tagged protein was detected with a Flag antibody (green). Ciliary axonemes (red) and cell membranes (blue) were visualized with an anti-acetylated antibody and an anti-GFP antibody, respectively. Scale bars: 10 µm.

E. Statistical analysis of the number of multiciliated cells per unit area in panels (**C)** and (**D).** Error bars represent the mean±s.d. P values were determined with the ordinary one-way ANOVA (P****<0.0001). Raw values were provided in source data file.

Figure 4. GJA1 depletion disrupts GRP cilium formation and left-right asymmetry.

A. GJA1-MO was injected into the dorso-vegetal blastomeres to target GRP tissues. Nodal cilium in the GRP were stained with an anti-acetylated tubulin antibody (green), and the cell membrane was

visualized by membrane-GFP, which was detected by an anti-GFP antibody (red). Scale bars: 20 µm.

B. The average lengths of GRP ciliary axonemes were plotted. Error bars represent the mean±s.d. P values were determined with the two-tailed t-test (P****<0.0001). Raw values were provided in source data file.

C-D. GJA1 depletion reversed heart looping in *Xenopus* embryos. Embryonic hearts were visualized by immunostaining with an anti-myosin heavy chain antibody (lower panel). GJA1 morphants displayed reversed heart looping. Approximately 30% of MO-injected embryos displayed reversed heart looping. Raw values were provided in source data file. Scale bars: 500 µm (upper-left panel), 100 µm (upper-right, lower panel). TA; truncus arteriosus, V; ventricle.

E–F. Expression of the left LPM-specific marker Pitx2 was disrupted in GJA1 morphants. Raw values were provided in source data file. Scale bars: 1 mm.

Figure 5. siRNA-mediated knockdown of GJA1 disrupts primary cilium formation in human RPE1 cells.

A. RPE1 cells were serum-starved for 24 hours and labeled with an anti-GJA1 antibody (green), an anti-acetylated tubulin antibody (red), and DAPI (blue). siRNA-mediated knockdown of GJA1 inhibited primary cilium formation, and the ciliary defects in human RPE1 cells were rescued by GJA1 transfection. Scale bars: 10 µm.

B. Statistical analysis of the percentage of ciliated cells in panel **(A)**. Error bars represent the mean±s.d P values were determined with the ordinary one-way ANOVA (P****<0.0001, P*=0.0238). Raw values were provided in source data file.

C. RPE1 cells were serum-starved for 24 hours and labeled with an anti-GJA1 antibody (green), an anti-acetylated tubulin antibody (red), and DAPI (blue). GJA1 was localized around the pericentriolar region in addition to gap junctions. Scale bars: 20 µm (left panel), 10 µm (right panel).

Figure 6. Knockdown of GJA1 results in the abnormal distribution of pericentriolar proteins involved in ciliogenesis.

A. RPE1 cells were transfected with GJA1 siRNA and immunostained with an anti-CP110 antibody

(green), an anti-acetylated tubulin antibody (red), and DAPI (blue). Two CP110 spots in both mother and daughter centrioles were observed in GJA1-depleted RPE1 cells. Scale bars: 20 µm (left panel), 5 µm (right panel).

B. The percentage of CP110 dots per cell in panel **(A).** Error bars represent the mean±s.d. P values were determined with the with the 2way ANOVA (P***=0.0004). Raw values were provided in source data file.

C. RPE1 cells were transfected with GJA1 siRNA and immunostained with an anti-BBS4 antibody (green) and an anti-acetylated tubulin antibody (red), and DAPI (blue). BBS4 puncta in the PCM were absent from the pericentriolar region of GJA1-depleted cells. The pericentriolar region is shown with higher magnification in the inset panels. Scale bars: 20 µm, 5 µm (inset).

Figure 7. Knockdown of GJA1 disrupted Rab11 trafficking to the ciliary base.

A. HA-tagged Rab11a was expressed in RPE1 cells, and the lysates were used for immunoprecipitation assays with GJA1 antibody-conjugated or IgG-conjugated beads. The immunoprecipitants were analyzed by immunoblotting with anti-GJA1 or anti-HA antibodies. Rab11a-HA was co-immunoprecipitated with endogenous GJA1.

B. RPE1 cells were serum-starved for 24 hours, and immunofluorescence staining analysis was performed with an anti-Rab11 antibody (green), an anti-GJA1 antibody (red), an anti-acetylated tubulin antibody (blue), and DAPI (gray). Rab11 and GJA1 accumulated around the pericentriolar-ciliary base. Scale bars: 5 µm.

C. GJA1-siRNA-treated RPE1 cells were immunostained with an anti-Rab11 antibody (green), an anti-GJA1 antibody (red), an anti-acetylated tubulin antibody (blue), and DAPI (gray). siRNA-mediated knockdown of GJA1 inhibited Rab11 accumulation around the pericentriolar region and basal bodies, and GJA1 transfection rescued the phenotype in RPE1 cells. Scale bars: 10 µm.

D. Statistical analysis of Rab11 accumulation in panel **(C).** Error bars represent the mean±s.d. P values were determined by one-way ANOVA (P^{***}=0.0008, P^{*}=0.0117). Raw values are provided in the source data file.

E–F. Super-resolution images of Rab11 localization. RPE1 cells were labeled with an anti-Rab11 antibody (green) and an anti-acetylated tubulin antibody (red). GJA1 depletion was not observed in Rab11-positive ciliary vesicles in the pericentriolar region. Images were obtained by SIM. Scale bars:

5 µm **(E)**, 1 µm **(F)**.

Figure 8. Dominant-negative mutant proteins of *Xenopus laevis* GJA1 fail to bind to Rab11.

A. HA-tagged Rab11a and WT-GJA1-Flag or dnGJA1-Flag were co-expressed in RPE1 cells, and the lysates were used for immunoprecipitation assays with anti-Flag antibody-conjugated beads. The immunoprecipitants were analyzed by immunoblotting with anti-Flag or anti-HA antibodies. Rab11a-HA co-immunoprecipitated only with WT-GJA1.

B. Statistical analysis of the relative Rab11a-HA binding affinity to WT-GJA1-Flag or dnGJA1-Flag mutant proteins in panel **(A)**. Error bars represent the mean±s.d. P values were determined by one-way ANOVA (P**=0.0050 (T154A, Δ130–136), P**=0.0025 (Δ234–243)). Raw values are provided in the source data file.

C. Suggested role of GJA1 during ciliogenesis. GJA1 is necessary for Rab11 positive vesicles trafficking to the vicinity of the basal bodies, thereby affecting CP110 removal to initiate ciliogenesis.

Figure 1

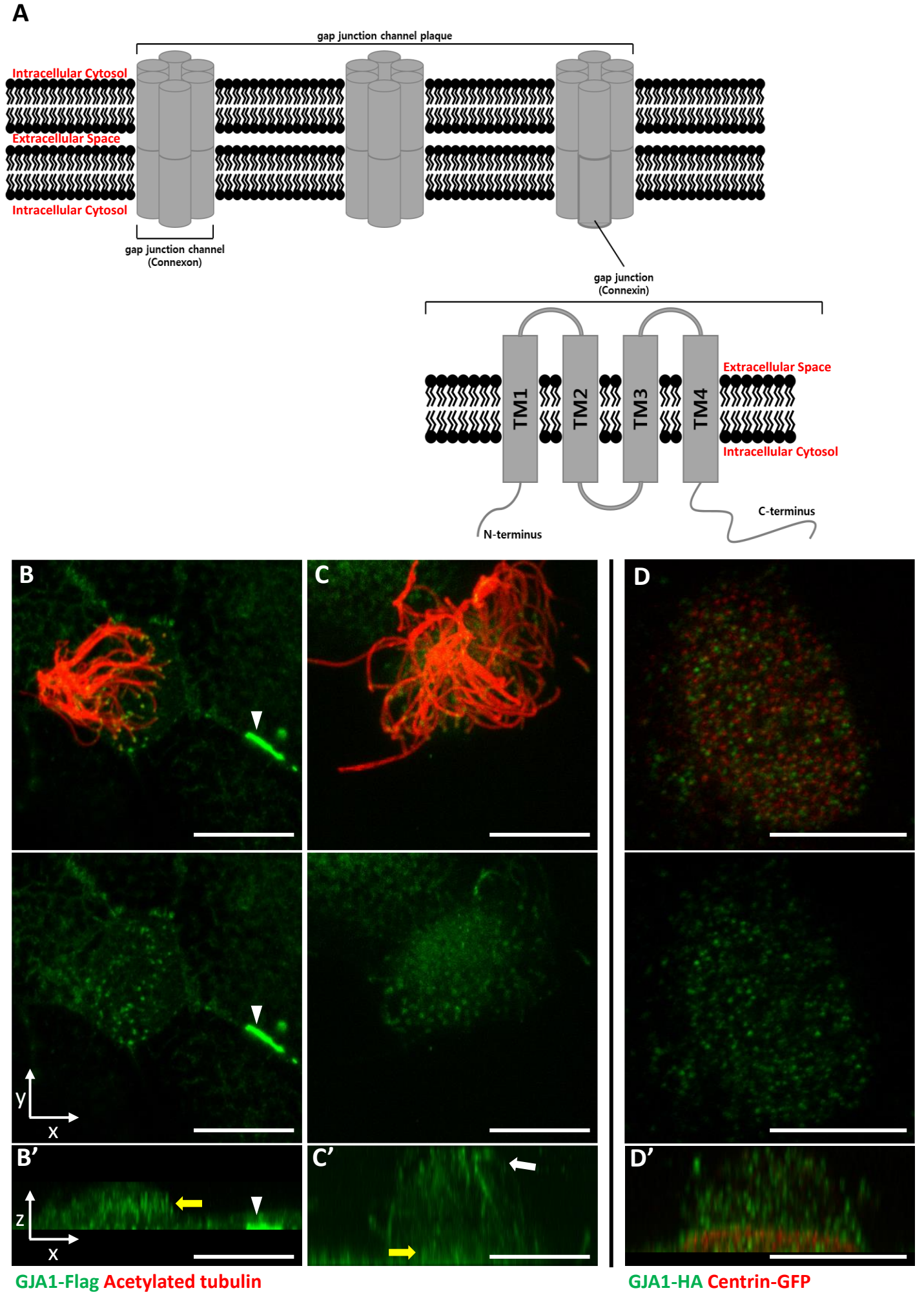
A
gap junction channel plaque
Intracellular Cytosol
Extracellular Space
Intracellular Cytosol
gap junction channel
(Connexon)
gap junction
(Connexin)
TM1
TM2
TM3
TM4
Extracellular Space
Intracellular Cytosol
N-terminus
C-terminus
B
C
D
y
x
B'
C'
D'
z
x
GJA1-Flag Acetylated tubulin
GJA1-HA Centrin-GFP

Figure 2

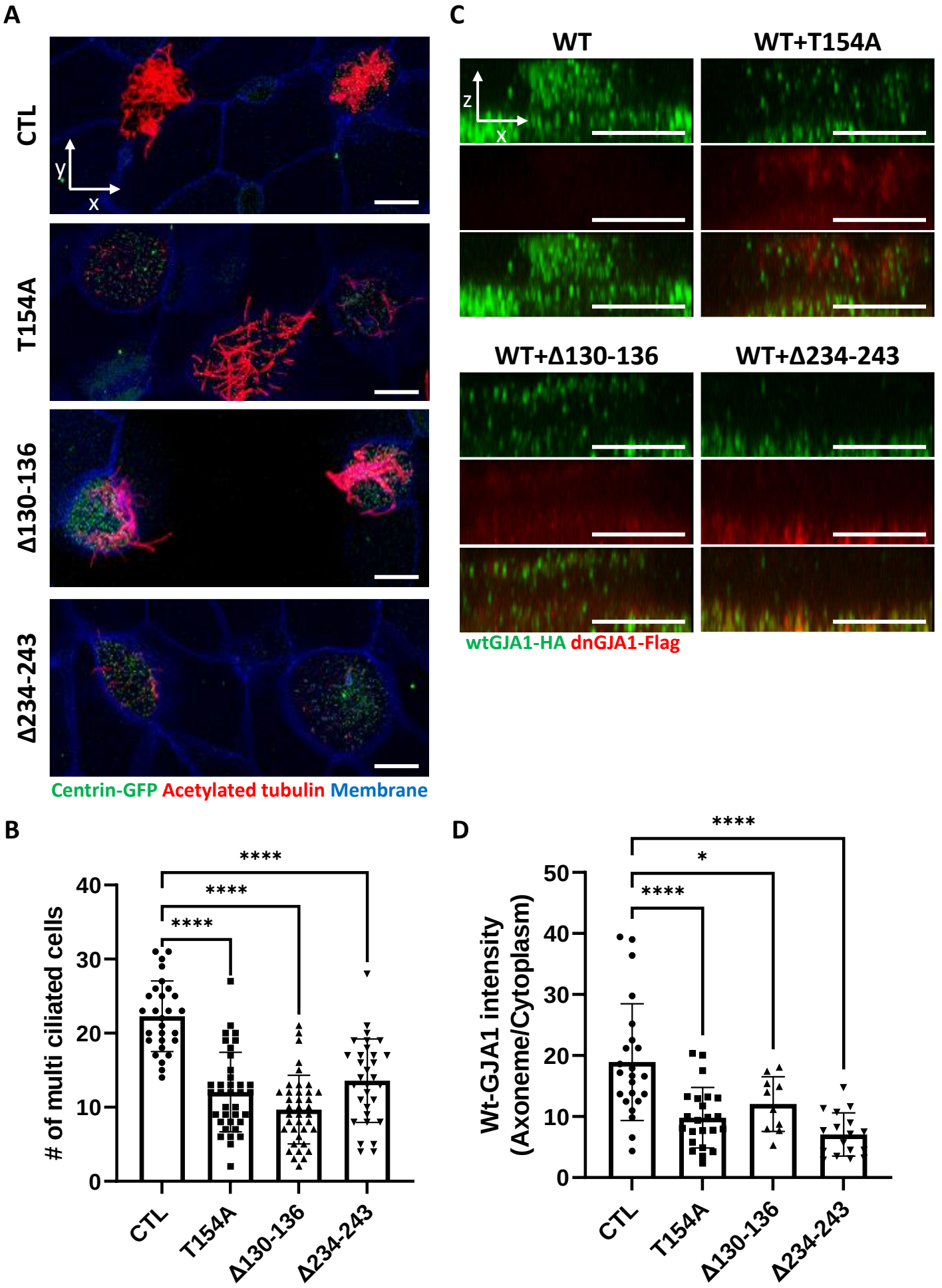
A
CTL
T154A
Δ130-136
Δ234-243
y
x
Centrin-GFP Acetylated tubulin Membrane
C
WT
WT+T154A
WT+Δ130-136
WT+Δ234-243
z
x
wtGJA1-HA dnGJA1-Flag
B
# of multi ciliated cells
0
10
20
30
40
****
****
****
CTL
T154A
Δ130-136
Δ234-243
D
Wt-GJA1 intensity
(Axoneme/Cytoplasm)
0
10
20
30
40
50
****
*
****
CTL
T154A
Δ130-136
Δ234-243

Figure 3

A

MO		+		+		+
GJA1-flag mRNA			Wt	Wt	Mis-m	Mis-m

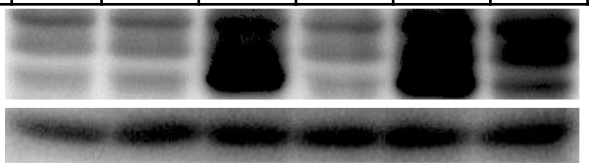

B

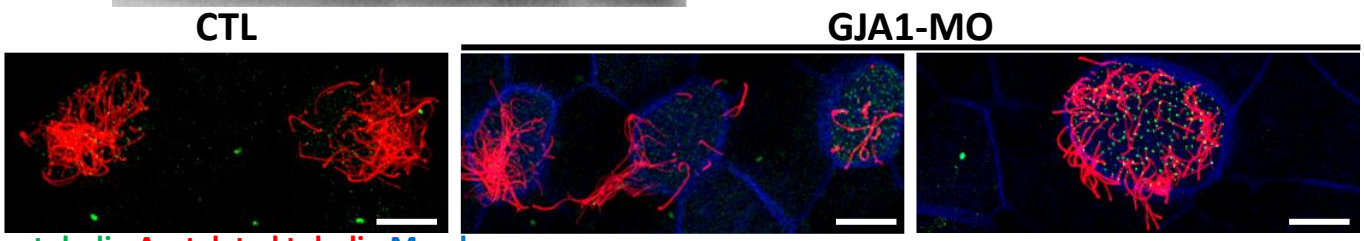

γ tubulin Acetylated tubulin Membrane

C

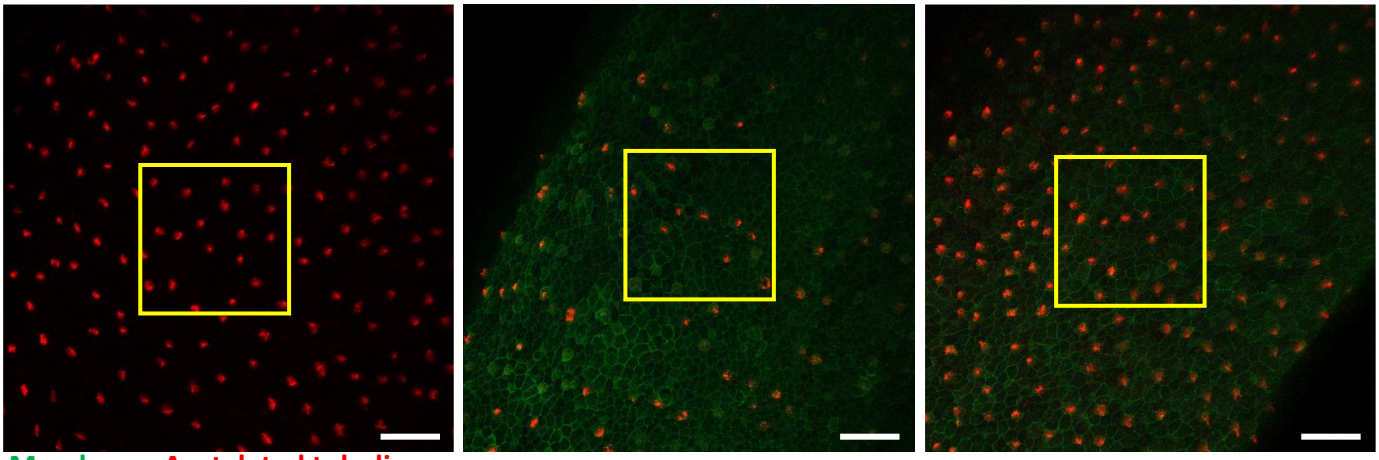

Membrane Acetylated tubulin

D

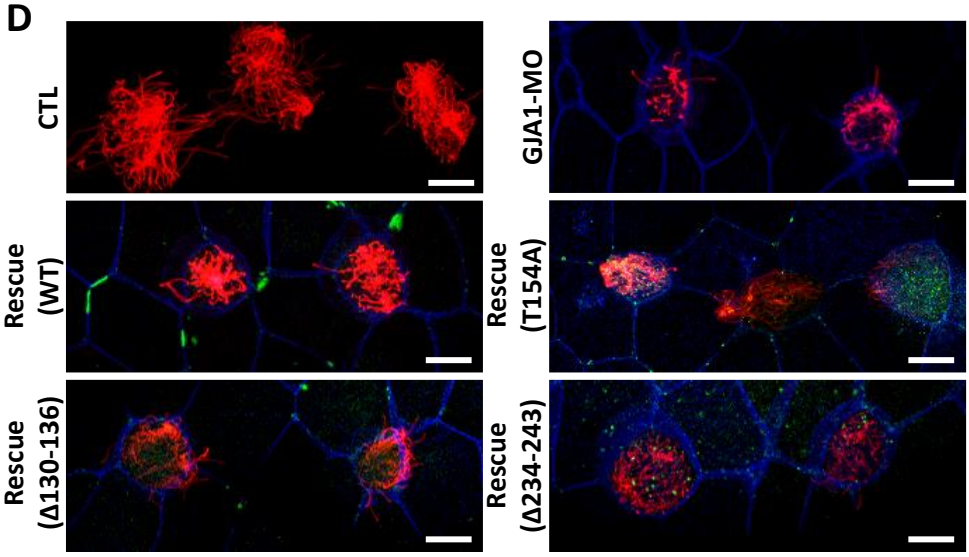

GJA1/dnGJA1-Flag Acetylated tubulin Membrane

E

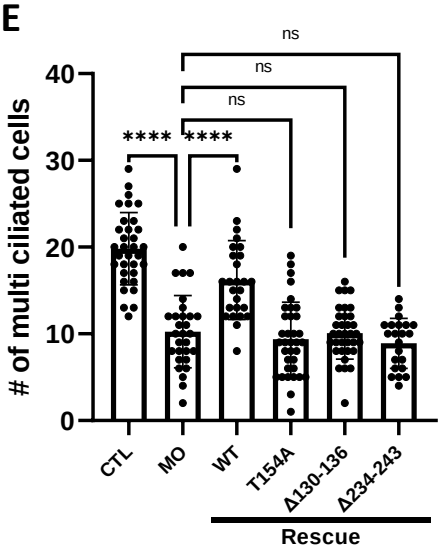

Figure 4

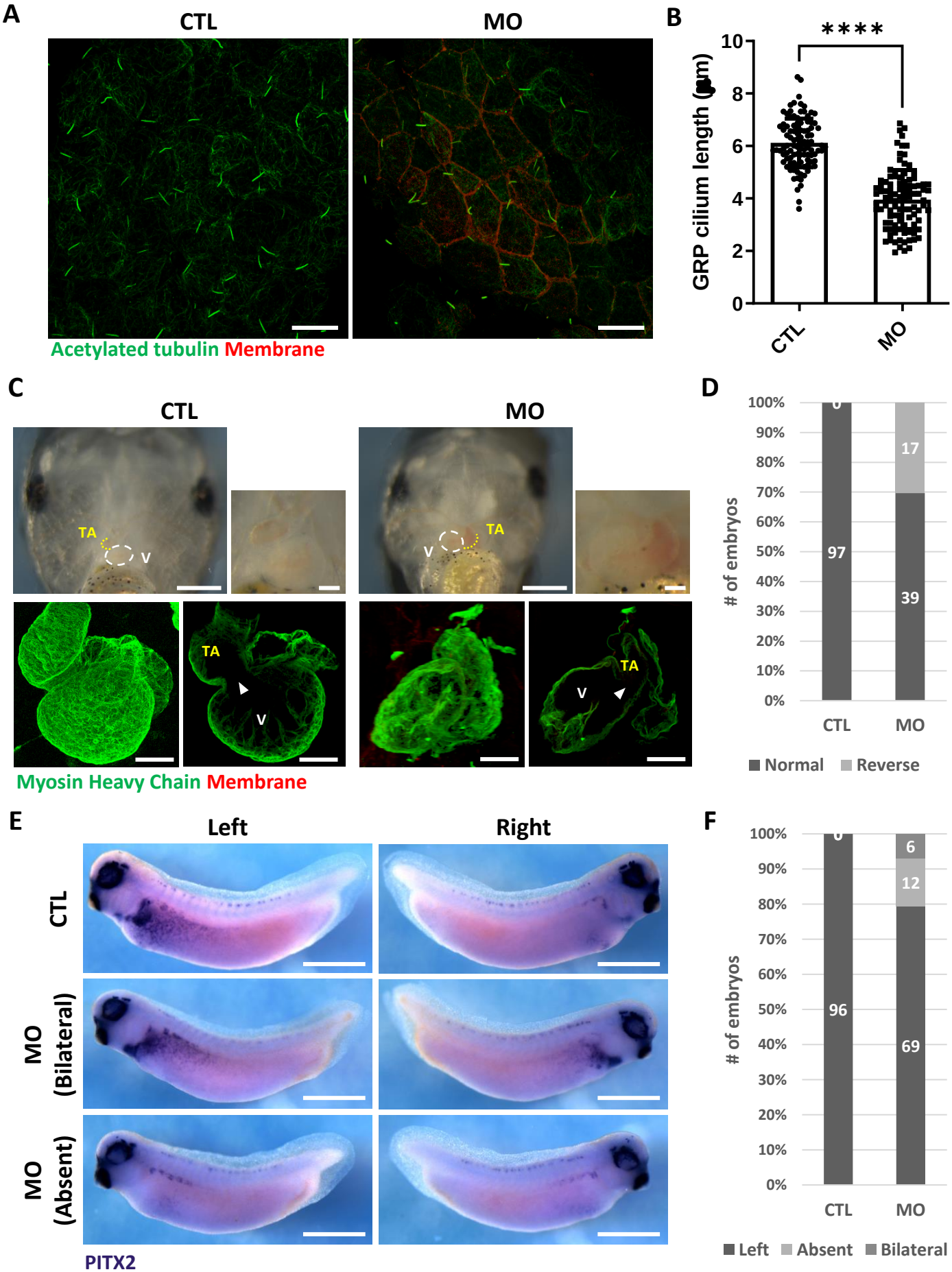
A
CTL
MO
Acetylated tubulin Membrane
B
****
GRP cilium length (µm)
10
8
6
4
2
0
CTL
MO
C
CTL
MO
TA
V
Myosin Heavy Chain Membrane
D
100%
90%
80%
70%
60%
50%
40%
30%
20%
10%
0%
# of embryos
0
17
97
39
CTL
MO
Normal
Reverse
E
Left
Right
CTL
MO (Bilateral)
MO (Absent)
PITX2
F
100%
90%
80%
70%
60%
50%
40%
30%
20%
10%
0%
# of embryos
0
6
12
96
69
CTL
MO
Left
Absent
Bilateral

Figure 5

A

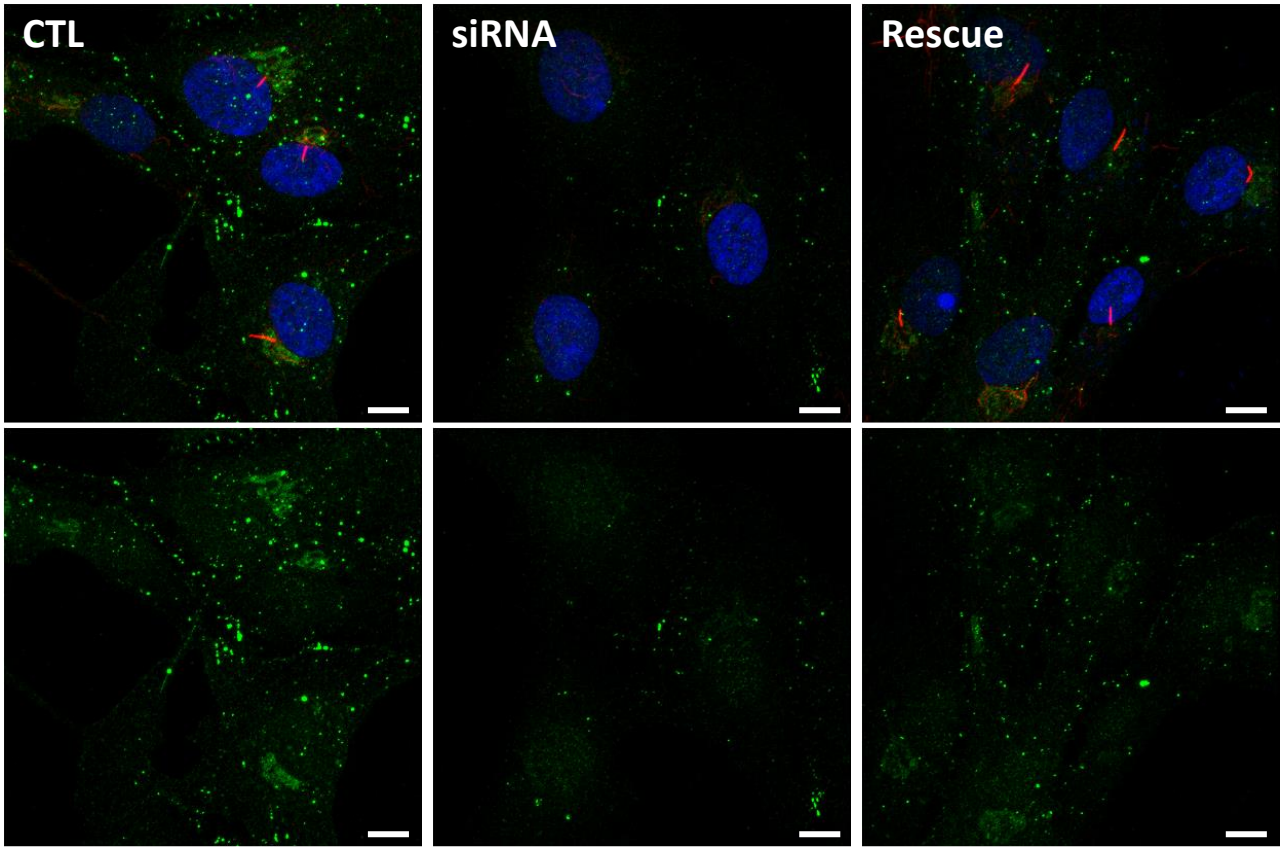

GJA1 Acetylated tubulin DAPI

B

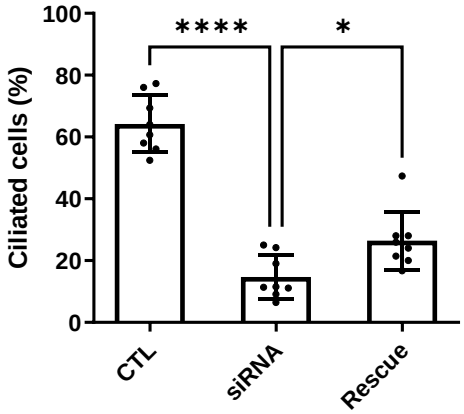

C

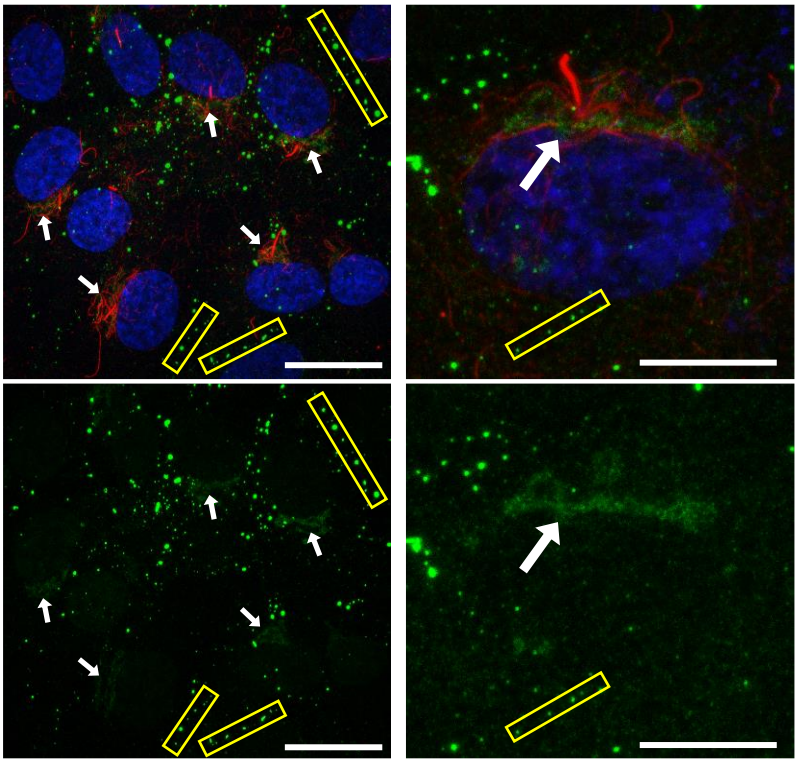

GJA1 Acetylated tubulin DAPI

Figure 6

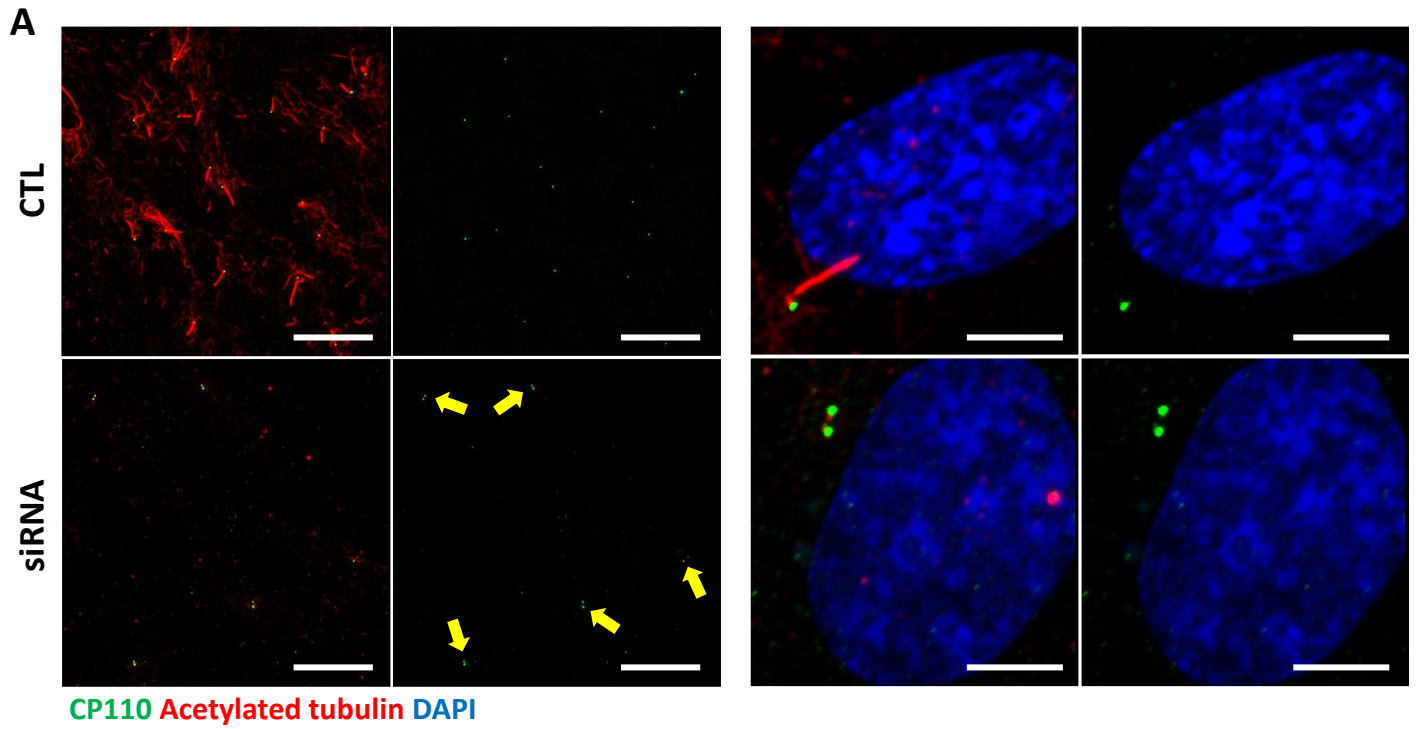
A
CTL
siRNA
CP110 Acetylated tubulin DAPI

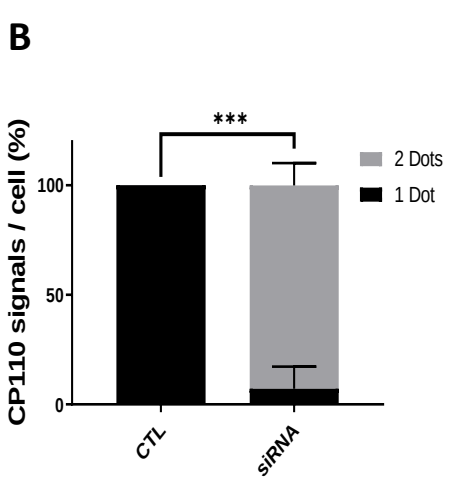
B
***
2 Dots
1 Dot
CP110 signals / cell (%)
100
50
0
CTL
siRNA

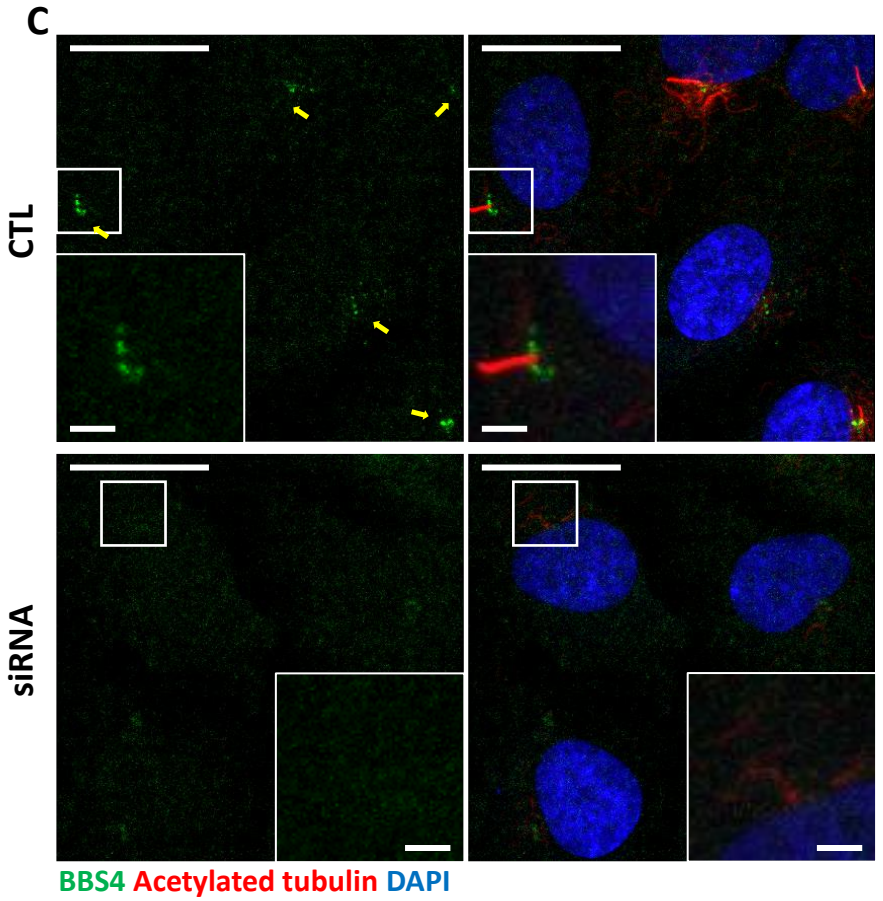
C
CTL
siRNA
BBS4 Acetylated tubulin DAPI

Figure 7

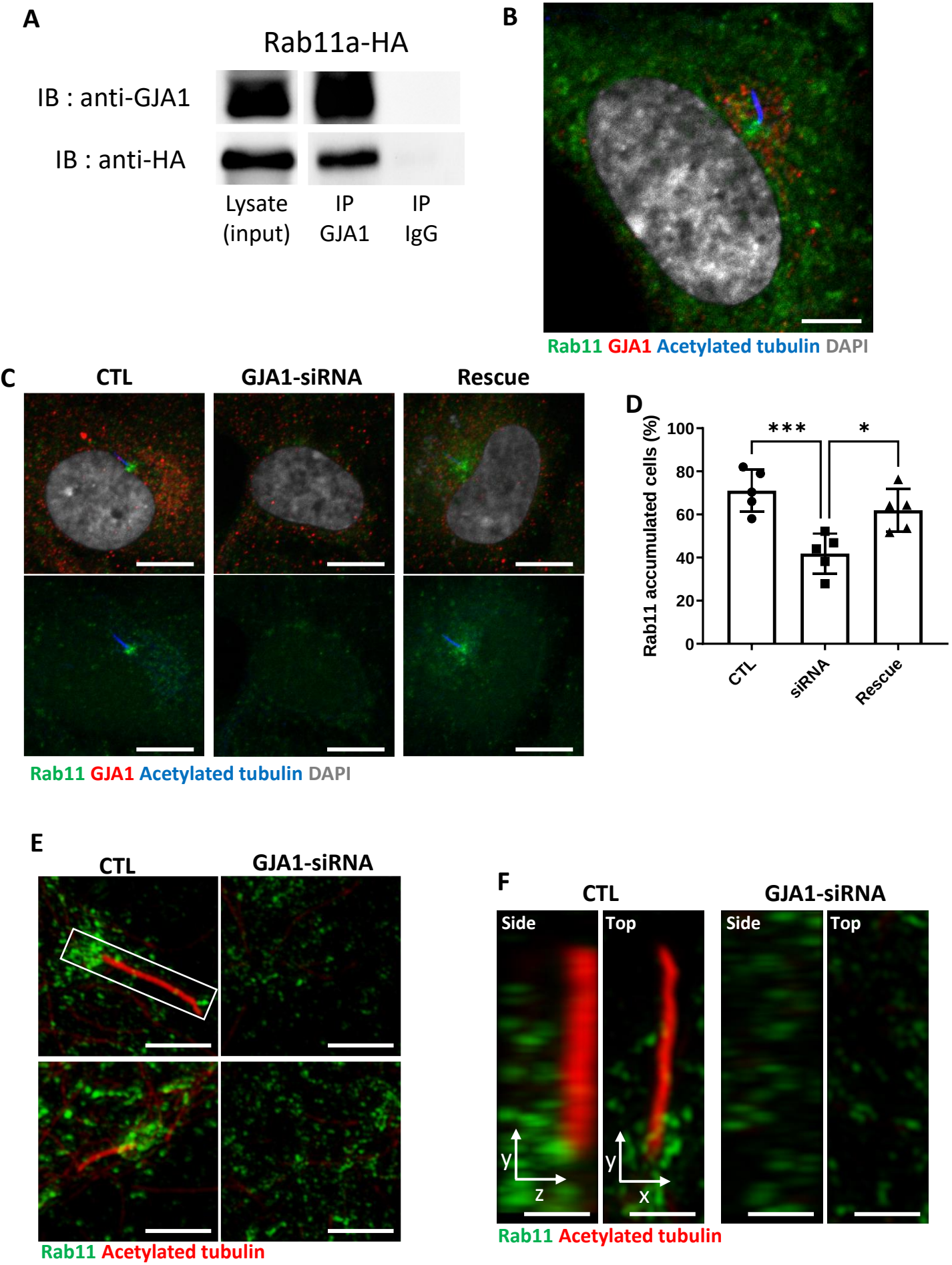
A
Rab11a-HA
IB : anti-GJA1
IB : anti-HA
Lysate (input)
IP GJA1
IP IgG
B
Rab11 GJA1 Acetylated tubulin DAPI
C
CTL
GJA1-siRNA
Rescue
Rab11 GJA1 Acetylated tubulin DAPI
D
Rab11 accumulated cells (%)
100
80
60
40
20
0
***
*
CTL
siRNA
Rescue
E
CTL
GJA1-siRNA
Rab11 Acetylated tubulin
F
CTL
GJA1-siRNA
Side
Top
Side
Top
y
z
y
x
Rab11 Acetylated tubulin

Figure8

A

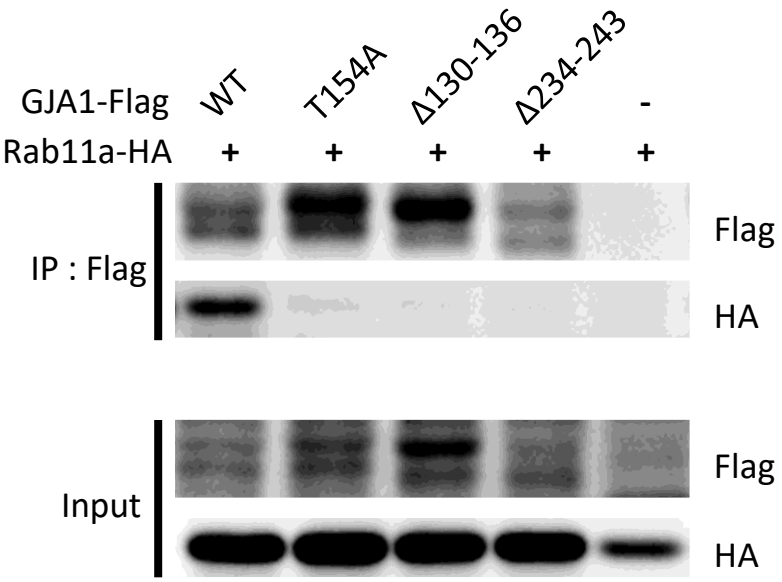
GJA1-Flag
WT
T154A
Δ130-136
Δ234-243
-
Rab11a-HA
+
+
+
+
+
IP : Flag
Flag
HA
Input
Flag
HA

B

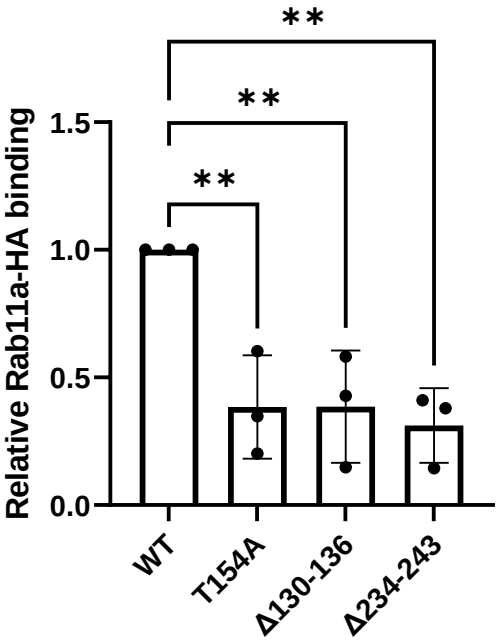
Relative Rab11a-HA binding
1.5
1.0
0.5
0.0
**
**
**
WT
T154A
Δ130-136
Δ234-243

C

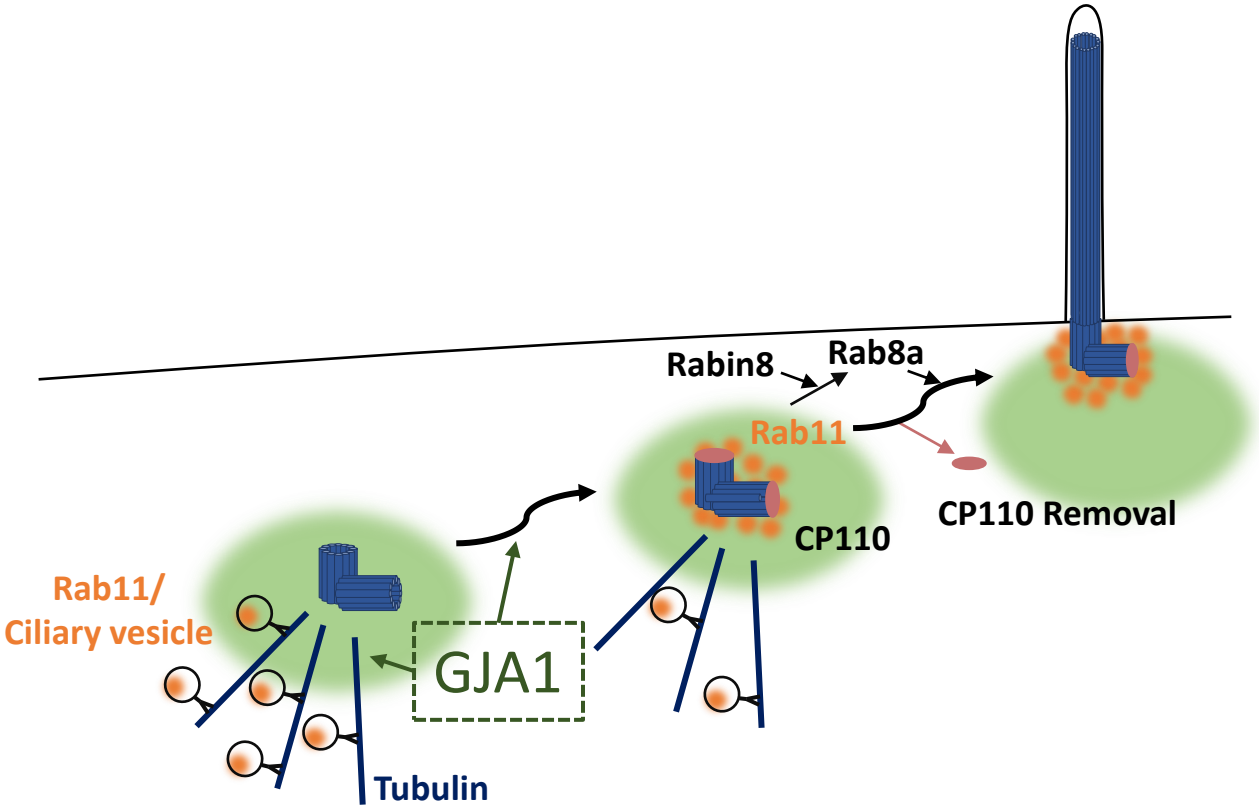
Rabin8
Rab8a
Rab11
CP110
CP110 Removal
Rab11/
Ciliary vesicle
GJA1
Tubulin